Cellular/Molecular

ISL1 and POU4F1 Directly Interact to Regulate the Differentiation and Survival of Inner Ear Sensory Neurons

Mei Xu,[1,2,3] Shuchun Li,[2] Xiaoling Xie,[2] Luming Guo,[1,2,3] Dongliang Yu,[4] Jiaping Zhuo,[2] Jacey Lin,[2] Lotem Kol,[2] and Lin Gan[2,5]

[1]College of Life Sciences, Zhejiang University, Hangzhou, Zhejiang 310058, China, [2]Department of Neuroscience and Regenerative Medicine, Augusta University, Augusta, Georgia 30912, [3]Institution of Life Sciences, Hangzhou Normal University, Hangzhou 310036, China, [4]College of Life Science and Medicine, Zhejiang Sci-Tech University, Hangzhou 310018, China, and [5]James and Jean Culver Vision Discovery Institute, Medical College of Georgia, Augusta University, Georgia 30912

The inner ear sensory neurons play a pivotal role in auditory processing and balance control. Though significant progresses have been made, the underlying mechanisms controlling the differentiation and survival of the inner ear sensory neurons remain largely unknown. During development, ISL1 and POU4F transcription factors are co-expressed and are required for terminal differentiation, pathfinding, axon outgrowth and the survival of neurons in the central and peripheral nervous systems. However, little is understood about their functional relationship and regulatory mechanism in neural development. Here, we have knocked out *Isl1* or *Pou4f1* or both in mice of both sexes. In the absence of *Isl1*, the differentiation of cochleovestibular ganglion (CVG) neurons is disturbed and with that *Isl1*-deficient CVG neurons display defects in migration and axon pathfinding. Compound deletion of *Isl1* and *Pou4f1* causes a delay in CVG differentiation and results in a more severe CVG defect with a loss of nearly all of spiral ganglion neurons (SGNs). Moreover, ISL1 and POU4F1 interact directly in developing CVG neurons and act cooperatively as well as independently in regulating the expression of unique sets of CVG-specific genes crucial for CVG development and survival by binding to the *cis*-regulatory elements including the promoters of *Fgf10*, *Pou4f2*, and *Epha5* and enhancers of *Eya1* and *Ntng2*. These findings demonstrate that *Isl1* and *Pou4f1* are indispensable for CVG development and maintenance by acting epistatically to regulate genes essential for CVG development.

Key words: **cochleovestibular ganglion (CVG); inner ear; LIM-homeodomain; POU-homeodomain; transcription factor**

Significance Statement

Inner ear neurons play critical roles in hearing and balance by transmitting auditory information in the form of electric signals from sensory hair cells to the brain. To study the genetic basis underlying their development, we identified the direct interaction and roles of transcription factors ISL1 and POU4F1 in regulating the development and maintenance of cochleovestibular ganglion (CVG) neurons. Moreover, our expression analysis uncovered that *Isl1* and *Pou4f1* are involved in the feedback regulation of CVG pioneer genes and control CVG differentiation genes. Furthermore, we identified and validated the function of the *cis*-regulatory elements bound by ISL1 and POU4F1 in vivo. Together, these findings provide insights into the gene regulatory network controlling the development of the inner ear neurons.

Received Sept. 12, 2023; revised Jan. 5, 2024; accepted Jan. 11, 2024.

Author contributions: M.X. and Lin Gan designed research; M.X., X.X., Luming Guo, J.Z., J.L., and L.K. performed research; M.X. and Lin Gan contributed unpublished reagents/analytic tools; M.X., S.L., and D.Y. analyzed data; M.X. and Lin Gan wrote the paper.

We thank Dr. Xiuqian Mu at the University of Buffalo for thoughtful discussion and assistance with CUT&Tag experiments and Drs. Min Deng and Ling Pan for technical assistance. We gratefully acknowledge the Genome Editing Core at Augusta University for generating the mouse models necessary to support this research and The Integrated Genomics Shared Resource in the Georgia Cancer Center for providing snATAC-Seq service. Lin Gan is supported by the NIH funding (DC008856 and DC021456), Augusta University Medical College of Georgia, and the Georgia Research Alliance.

The authors declare no competing financial interests.

Correspondence should be addressed to Lin Gan at ligan@augusta.edu.

https://doi.org/10.1523/JNEUROSCI.1718-23.2024

Introduction

The mammalian inner ear consists of auditory and vestibular systems responsible for hearing and balance, respectively (Torres and Giráldez, 1998). Among the diverse cell types in the inner ear, hair cells and sensory ganglion neurons play key roles in hearing and balance function and their dysfunction results in sensorineural hearing loss (SNHL) (Fettiplace and Hackney, 2006). While hearing aids and cochlear implants improve the hearing abilities by amplifying the received sound (NIDCD, 2013) or stimulating the sensory neurons electrically (NIDCD, 2016), these therapies fundamentally rely on functional sensory

neurons. The protection and regeneration of sensory neurons provide therapeutic strategies that support hearing restoration. Therefore, it is essential to identify and characterize the gene regulatory network (GRN) of sensory neuron development.

In the mouse inner ear, sensory neurons originate from neuroblasts delaminating from the ventral region of the otic vesicle (Kelley, 2006; Appler and Goodrich, 2011). Once delaminated, the neuroblasts coalesce adjacent to the developing inner ear to form cochleovestibular ganglion (CVG) neurons. As development continues, CVG neurons segregate to form spiral ganglion neurons (SGNs) and vestibular ganglion neurons (VGNs). These processes are highly controlled by a hierarchical network of transcription factors (TFs). SIX1 and EYA1, both crucial neuronal determination factors, interact directly to drive neurogenesis and cooperate with SOX2 to regulate auditory neuron differentiation (Ahmed et al., 2012; Steevens et al., 2019). With the downstream of these TFs, the basic helix-loop-helix (bHLH) TF NEUROG1 is required for the initial specification of neuronal precursors (Ma et al., 1998, 2000) and NEUROD1, another bHLH TF downstream of NEUROG1, is necessary for the differentiation and maintenance of auditory neurons (Kim et al., 2001). Besides bHLH TFs, other TFs play important roles in the development of CVG neurons. For example, POU4F1, a Class IV POU-homeodomain TF, is required for the development of CVG neurons, including regulating terminal differentiation, mediating pathfinding, promoting axon outgrowth and cell survival (Ryan, 1997; Huang et al., 2001; Sherrill et al., 2019). Though POU4F1 plays a pivotal role in regulating CVG development, only about 30% SGNs are lost in *Pou4f1KO* mice (Huang et al., 2001), suggesting that additional factors could be required for regulating the development of CVG. ISL1, a LIM-homeodomain (LIM-HD) TF, is essential for the differentiation of a variety of neurons, including motor neurons (Pfaff et al., 1996), trigeminal ganglion (TG) neurons and dorsal root ganglion (DRG) neurons (Sun et al., 2008), and retina ganglion cells (RGCs) (Mu et al., 2008; Pan et al., 2008). ISL1 and POU4F1 are mostly co-expressed in developing CVG neurons whereas the onset of ISL1 expression slightly precedes that of POU4F1 (Deng et al., 2014), suggesting a functional interaction of these two TFs in CVG neurons. More importantly, a published study has shown that *Pou4f1* and *Isl1* act epistatically to regulate the gene expression program of sensory differentiation in DRG (Dykes et al., 2011). Collectively, these studies suggested that *Isl1* and *Pou4f1* could act together to regulate the development of the inner ear neurons.

To assess the function of ISL1 and POU4F1, we carried out the inner ear-specific knock-out of *Isl1* and *Pou4f1* using *Pax2*-Cre (Ohyama and Groves, 2004). We found that deletion of *Isl1* alone resulted in profound defects in CVG development and axon pathfinding of SGNs. Additionally, deletion of both *Isl1* and *Pou4f1* caused more severe CVG defects, with nearly complete ablation of SGNs. Transcriptome analysis by next-generation sequencing (NGS) revealed that the loss of *Isl1* or *Pou4f1* or both resulted in a broad change in the expression of genes involved in axon guidance, axonogenesis, and other neurodevelopmental pathways. Moreover, our analyses of ISL1-POU4F1 interaction, CUT&Tag, snATAC-Seq and in vivo enhancer deletion identified the downstream effector genes that ISL1 and POU4F1 directly bind to and regulate in the developing CVG neurons. Our results demonstrate that *Isl1* and *Pou4f1* act epistatically to regulate the differentiation and survival of auditory neurons and reveal the underlying molecular mechanisms of their direct interaction during neurogenesis.

Materials and Methods

Mice. The *Pou4f1KO*, *Isl1*^{lacZ}, *Isl2*^{V5}, and *Isl1*^{loxP} mice lines were generated in our laboratory and have been described previously (Xiang et al., 1996; Elshatory et al., 2007; Pan et al., 2008). All of the analyses were conducted in mice of either sex ($n \geq 3$ for each genotype). *Tg(Pax2-cre)1Akg* transgenic mice express Cre recombinase throughout the inner ear, the midbrain, the cerebellum, the olfactory bulb, and the kidney (Ohyama and Groves, 2004) and have been used previously as an effective inner ear-specific deleter (Chang et al., 2008; Luo et al., 2013). Thus, *Pax2-Cre* transgenic mice were used to specifically delete *Isl1* in the inner ear during developmental stages (Hayashi and McMahon, 2002; Ohyama and Groves, 2004). Embryos were identified as E0.5 at noon on the day at which vaginal plugs were observed. Mice of both sexes were used in this study. All animal procedures used in this study were approved by Institutional Animal Care and Use Committee (IACUC) at Augusta University.

Immunohistochemistry, X-Gal staining, BrdU pulse labeling, in situ hybridization, and RNAScope. Based on their developmental stages, embryos or heads of postnatal mice were fixed in 4% paraformaldehyde (PFA) in phosphate-buffered saline (PBS, pH7.2) at 4°C for different times. After three washes of PBS, the tissues were dehydrated in 20% sucrose in PBS at 4°C overnight, embedded in O.C.T. compound (Tissue-Tek, Sakura Finetek), and cryosectioned at a thickness of 14–20 µm. Immunolabeling of the sections was then conducted as previously described (Deng et al., 2010; Luo et al., 2013). Primary antibodies and concentrations used for this study were: mouse anti-POU4F1 (1:200, Santa Cruz Biotechnology (SCBT), Inc.), goat anti-POU4F2 (SCBT, 1:200), rabbit anti-Caspase-3 (1:500, R&D Systems, Inc.), rabbit anti-ISL1 (1:500, Developmental Studies Hybridoma Bank), goat anti-NEUROD1 (SCBT, 1:200), rabbit anti-GATA3 (1:500, ab199428, Abcam PLC.), and goat-anti TRKC (R&D, 1:100). Alexa-conjugated secondary antibodies were obtained from Molecular Probes and were used at a dilution of 1:1,000. Images were captured with a Zeiss 710 META confocal microscope or Leica STELLARIS confocal.

Detection of β-galactosidase activity was determined by X-Gal staining (Gan et al., 1999). Briefly, embryos were fixed in 4% PFA in PBS at 4°C for 1 h. Whole-mount embryos or 20 µm frozen sections were stained overnight at room temperature with 0.1% X-Gal, 5 mM potassium ferricyanide, 5 mM potassium ferrocyanide, and 2 mM $MgCl_2$ in PBS.

For bromodeoxyuridine (BrdU) (Sigma) pulse-labeling experiments, pregnant females were injected intraperitoneally with 100 µg BrdU/gram body weight 1 h before they were sacrificed. Embryo were dissected out at E10.5 and E11.5, fixed in 4% PFA for 4 h, cryosectioned at 14 µm thickness, and stained with mouse anti-BrdU antibody (Becton Dickson, 1:200) following the regular immunolabeling procedure. Finally, the BrdU signals were visualized by Alexa-conjugated anti-mouse secondary antibody under confocal microscope.

For section in situ hybridization, embryos were dissected out in PBS, fixed in ice cold 4% PFA in PBS, dehydrated with gradient sucrose, embedded in O.C.T. medium (Tissue-Tek), and sectioned at 20 µm thickness. Hybridization was carried out with specific digoxigenin-labeled RNA probes and detection was done with anti-CIP/NBT color development as previously described (Li and Joyner, 2001).

For RNAScope detection of gene expression, E11.5 embryos were collected and fixed in ice cold 4% PFA in PBS, dehydrated with gradient sucrose, embedded in O.C.T. medium (Tissue-Tek), and sectioned at 16 µm thickness. Sections were subjected to a combination of IHC labeling and RNAScope in situ hybridization following the instruction of "RNAScope Multiplex Fluorescent v2 Assay Combined with Immunofluorescence: Integrated Co-Detection Workflow (ICW)" (MK 51-150) from Advanced Cell Diagnostics. Briefly, the sections were blocked, target retrieved, and then labeled with primary antibody followed by proteinase treatment and hybridization with probe. After that, signals were amplified on sections and probes were labeled with respective channels. Lastly, sections were treated with secondary antibodies, mounted and imaged under a Leica STELLARIS confocal microscope. *Myt1* probe was obtained from Advanced Cell Diagnostics (S1047201-C2).

Neuronal tracing. These experiments were performed as described previously (Fritzsch, 2003; Fritzsch et al., 2005). The PFA-fixed heads of embryos or postnatal mice were sagittally cut at the midline into two halves, filter strips with lipophilic dye were inserted into the brainstem or the cerebellum. The samples were then incubated at 37°C in 4% PFA. After appropriate length of incubation when the dye had diffused into the fine terminals, inner ears were dissected and flat-mounted in glycerol. Inner ears were imaged with a Nikon E800 using a Bio-Rad 2000 confocal system or a Zeiss LSM 510 confocal system (Maklad and Fritzsch, 2002).

Proximity ligation assay (PLA). For PLA, E10.5 embryos were dissected out and fixed in 4% PFA at 4°C for at least 2 h, then washed with PBS three times, dehydrated with gradient sucrose, embedded in O.C.T. medium, and sectioned at 5–10 µm thickness. PLA assay was performed with Duolink PLA kit (DUO92101, Millipore Sigma) according to the manufacturer's instruction. Briefly, on day 1, the slides were warmed at 37°C for 1 h, and then 1 drop (~40 µl) of Duolink Blocking Solution was applied to each section. After the slides were incubated at 37°C for 1 h in a humidity chamber, Duolink Blocking Solution was tapped off. Primary antibodies diluted in the Duolink Antibody Diluent (rabbit anti-ISL1, Abcam#ab20670, 1:1,000 and mouse anti-POU4F1, Millipore#MAB1585, 1:1,000) were added to the sections and slides were incubated at 4°C overnight. On day 2, slides were washed twice with Wash Buffer A for 5 min each at room temperature. Diluted PLA PLUS and MINUS probe solutions (1:5 dilution in Duolink Antibody Diluent) were applied, and slides were incubated at 37°C for 1 h in a humidity chamber. Afterwards, slides were washed twice with Wash Buffer A for 5 min each at room temperature and were treated in ligation solution (1:8:31 ligase:5× Duolink Ligation buffer:water) at 37°C for 30 min in a humidity chamber. After two washes as above in Wash Buffer A, the slides were incubated in Amplification buffer (1:16:63 polymerase:5× Amplification buffer:water) in the humidity chamber for 100 min at 37°C. Finally, the slides were washed twice in 1× Wash Buffer B for 10 min each at room temperature and once in 0.01× Wash Buffer B for 1 min and mounted in Duolink-In Situ Mounting Medium with DAPI for 15 min before analyzing under a Leica STELLARIS confocal microscope.

RNA-Seq and qRT-PCR. For each pair of replicates, CVG neurons at E11.5 were dissected out from nine embryos of each genotype and frozen in liquid nitrogen immediately. The fresh frozen CVG neurons in Trizol were shipped to Azenta Life Science to perform RNA extraction, library preparation and sequencing. Briefly, total RNA was extracted using Trizol (ThermoFisher Scientific) following the manufacturer's protocol. The RNA-Seq libraries were prepared using NEBNext Ultra II Directional RNA Library Prep Kit (NEB) following the manufacturer's instruction. Sequencing was performed on Hiseq 4000 (Illumina, Inc.) with 2 × 150 bp paired-end reads and the depth was 20–30 million reads per sample. Low quality sequencing reads were filtered and trimmed with the Trimmomatic software. The quality of sequence reads was evaluated using the FASTQ analysis, following which the high-quality sequence reads were aligned to the mouse mm10 reference transcriptome using the HISAT2. The HISAT2 outputs were converted with SAMtools and then loaded into StringTie for transcript quantification. Finally, the count tables or matrices were input into the LEPSeq statistical package to determinate the differential expression gene between controls and mutants (cutoff fold-change >2 and adjusted p value <0.05). Genes of clusters were selected to perform cluster heatmap and GO terms analysis (https://www.bioinformatics.com.cn/srplot). The accession number for the RNA-Seq data is GSE233755.

For qRT-PCR, CVG neurons from six embryos of each genotype at E11.5 were isolated under microscopy and collected into tubes with 350 µl Lysis Buffer provided by the RNeasy Mini Kit (Qiagen). Then total RNA was extracted following the manufacturer's instruction and resuspended in 30 µl RNase-free water. cDNA was synthesized with iScript cDNA Synthesis Kit following the manufacturer's instruction and measured by Nanodrop 2000. qPCR was run with SsoAdvanced Universal SYBR Green Supermix (Bio-Rad) following the manufacturer's instruction on CFX96 PCR System. *Actb* was used as the housekeeping gene control. The primers are listed in Extended Data Table 5-1.

CUT&Tag. The CUT&Tag experiment was performed using reagents and protocol provided by EpiCypher, Inc. with minor modifications (Ge et al., 2023). E11.5 CVGs were isolated and nuclei were extracted immediately by incubating in the NE Buffer for 10 min on ice. For each experiment, greater than 1×10^5 nuclei were used. The nuclei were incubated with the activated Concanavalin A-coated magnetic beads (11 µl/sample, EpiCypher #21-1401) at room temperature for 10 min. The nuclei-beads were collected using magnetic stand and resuspended in 50 µl ice cold Antibody Buffer. 0.5 µg antibody against ISL1 (rabbit, AB4326, Millipore; rabbit, ab20670, Abcam), POU4F1 (mouse, MAB1585, Millipore), H3K27ac (EpiCypher #13-0045), H3K27me3 (C15410195, Diagenode), H3K4me3 (EpiCypher #13-0041), or control IgG (mouse, C15400001, Diagenode; rabbit, EpiCypher #13-0042) was added to each sample and mixed on a rotator at 4°C overnight or at room temperature for 2 h. The antibody-bound nuclei-beads were isolated and resuspended in 50 µl of ice cold Digitonin 150 Buffer. 0.5 µg of anti-rabbit or anti-mouse IgG secondary antibody (EpiCypher #13-0047 and #13-0048) was added and samples were incubated for 30 min at room temperature on a rotator. After two washes in ice cold Digitonin 150 Buffer, nuclei-beads were resuspended in 50 µl of ice cold Digitonin 300 Buffer, 2.5 µl of CUTANA pAG-Tn5 solution (EpiCypher #15-1017) was added, and nuclei-beads were incubated for 1 h at room temperature on a rotator. The samples were again washed twice in ice cold Digitonin 300 Buffer, resuspended in 125 µl of cold Tagmentation Buffer, and incubated at 37°C for 1 h. Then, 2.5 µl of 0.5 M EDTA, 1.25 µl of 10% SDS and 1.1 µl of 20 mg/ml Proteinase K were added to each sample and samples were incubated at 70°C for 10 min or 55°C for 30 min. After this, DNA fragments were purified and collected in 30 µl of ddH_2O using Cycle Pure Kit (Omega, D6492-02) following the manufacturer's instruction. To prepare the library, 21 µl of DNA fragments were transferred to a PCR tube, to which 2 µl of barcoded i5 and i7 primers and 25 µl CUTANA High Fidelity 2× PCR Master Mix (EpiCypher, #15-1018) were added. PCR was performed using the following conditions: 72°C for 5 min, 98°C for 30 s, and 20 cycles of 10 s at 98°C and 10 s at 63°C, followed by an extra 1 min extension at 72°C. The PCR product was analyzed on an Agilent Fragment Analyzer. Combined DNA libraries were cleaned up using AMPure XP beads (#A63880, Beckman Coulter) following the manufacturer's instructions. Each pooled DNA library of 10 samples was resuspended into 40–80 µl water and quantified using the NanoDrop (Thermo Scientific). Library fragments were sent for sequencing commercially at Azenta Life Science. Sequencing was performed on Hiseq 4000 (Illumina) with 2 × 150 paired-end reads and a depth of 10 million reads per sample. Each antibody had two or more replicates. Raw data of each replicate was analyzed following the CUT&Tag Data Processing and Analysis Tutorial (https://yezhengstat.github.io/CUTTag_tutorial/). Briefly, raw data was pre-processed for quality control using FastQC. Qualified peaks were aligned to the mouse mm10 reference transcriptome using the Bowtie2. Peaks were called using MACS2 and SEACR. At last, peak annotation and functional analysis were performed using ChIP seeker and visualized by IGV. The accession number for the CUT&Tag-Seq data is GSE233840.

snATAC-Seq. Cochleae of C57BL/6J embryos at E12.5 were isolated in cold PBS and nuclei were immediately isolated according to 10× Genomics protocols (CG000375 Rev C) without FACS sorting. The libraries for Chromium Single Cell Multiome ATAC + Gene Expression were produced exactly as written (CG000338 Rev A, 10× Genomics Inc.) and sequenced using Illumina Novaseq 6000 S1 (100 cycles, 2 × 50 pair ending). Sequences were aligned to the Ensembl mouse mm10 assembly using CellRanger-ARC-2.0.0 (10× Genomics) analysis software. After removing doublets with AMULET (Thibodeau et al., 2021) for snATAC data and scDblFinder (Germain et al., 2021) or scRNA data, quality control (QC) of single-nuclei transcriptome and chromatin profiles were conducted by Seurat (v4.3.0) in R package (v4.2.2). Weighted nearest neighbors (WNN) (Hao et al., 2021) were

applied to integrate batch-effect corrected (Harmony (Korsunsky et al., 2019)) snRNA-Seq and snATAC-seq data. Cells with expression of *Nrxn1* and *Sox2* were selected as spiral ganglion cells and prosensory cells, respectively. The accession number for the snATAC-Seq data is GSE233706.

Enhancer deletion by genome editing with CRISPR/Cas9 in mice. To delete the selected enhancers, two single guide RNAs (sgRNAs) flanking each peak region were identified using CRISPOR (Concordet and Haeussler, 2018) and synthesized by Synthego Corp. The sgRNAs and Cas9 protein (Alt-RS. p. Cas9 Nuclease V3 from Integrated DNA Technologies, Inc.) were introduced into C57BL/6J zygotes (Jackson Laboratory, stock#009086) by electroporation. The zygotes were then transferred into pseudopregnant Swiss recipient mice. Embryos were collected at E11.5 and embryos with homozygous deletion were verified by PCR genotyping and Sanger sequencing. Wild-type control and homozygous deletion littermates were selected for expression analysis by in situ hybridization. Sequences of sgRNAs and PCR genotyping primers used in this study are shown in Extended Data Table 8-1.

Quantification and statistical analysis. Statistical analyses of apoptotic cell numbers were performed by using a two-tailed Student *t* test to determine the differences. Due to the morphologically disorganized mutant tissues and lack of clear demarcation of early CVG, we averaged the counts of the $CASP3^+$ cells in CVG per section for the $CASP3^+$ cell quantification. For each E11.5 to E13.5 specimen, four to six serial sections were co-labeled with anti-CASP3 and anti-NEUROD1 (to mark the CVG). For each E14.5 specimen, six to eight serial sections were co-labeled with anti-CASP3 and anti-TUJ1 (to mark SG and VG). Once segregated, SGNs are in different sectional levels from VGNs. We analyzed six embryos for each group and compared the number of $CASP3^+$ cells for CVG, SG, and VG separately. To quantify the changes in the number of $NEUROD1^-/ISL1/2^+$ postmitotic CVG neurons in the central CVG region, we have analyzed more than three embryos of each group and performed ANOVA analysis. All graphs are constructed via Prism 6.0.

Results

Isl1 inactivation leads to defective SGNs and VGNs

To investigate the role of *Isl1* in CVG development, we used two modified *Isl1* alleles: a conditional knock-out allele ($Isl1^{loxP}$) and a nuclear *lacZ* reporter knock-in allele ($Isl1^{lacZ}$) (Pan et al., 2008). We first analyzed the spatiotemporal expression of *Isl1-lacZ* knock-in reporter in developing inner ear neurons of $Isl1^{lacZ/+}$ heterozygous mice by X-Gal staining for β-galactosidase activity. Consistent with previous studies of *Isl1* expression (Radde-Gallwitz et al., 2004; Deng et al., 2014), *Isl1-lacZ* expression was detected in all delaminated and migrating CVG neurons as well as in facial ganglion (FG) cells at E10.5–E12.5 (Fig. 1*A*). In SGNs, *Isl1-lacZ* expression was strong at E13.5 and persisted to adulthood (Fig. 1*A*). In addition to the high expression level in SGNs, strong *Isl1* expression was also detected in VGNs as well as in the saccule, utricle, and crista (Fig. 1*A*). Collectively, these results indicate that *Isl1* is continuously expressed in early CVG neurons as well as mature SGNs and VGNs.

To investigate the impact of *Isl1* deletion on CVG development, we crossed $Isl1^{loxP}$ and $Isl1^{lacZ}$ mice with *Tg(Pax2-Cre)* mice, which express Cre recombinase throughout the inner ear, midbrain, cerebellum, olfactory bulb, and kidney (Ohyama and Groves, 2004), to generate *Isl1* conditional knock-out ($Isl1^{loxP/lacZ}$; *Pax2-Cre*, hereafter referred to as *Isl1CKO*) mice to specifically delete *Isl1* in the inner ear. We evaluated the efficiency of inner ear-specific *Isl1* inactivation by *Pax2*-Cre using immunolabeling with anti-ISL1 antibody, which recognizes both ISL1 and ISL2 in neurons of CVG and FG. Compared to the control, there was a significant reduction of proliferating CVG cells positive for anti-ISL1 immunolabeling in the *Isl1CKO*, while the postmitotic neurons in the central CVG remained positive for anti-ISL1 immunolabeling (Fig. 1*B*). These postmitotic neurons in the central CVG expressed ISL2 and were NEUROD1-negative (Fig. 1*C*), suggesting that the anti-ISL1 labeling signal detected in the central CVG of the *Isl1CKO* inner ear should result from the expression of ISL2 but not of ISL1. Consistently, quantitative RT-PCR of *Isl1* mRNA using primers in exons 2 and 3 demonstrated that *Isl1* mRNA expression was specifically ablated in the developing inner ear of *Isl1CKO* embryos (Fig. 1*D*).

In contrast to control $Isl1^{lacZ/+}$ inner ears in which X-Gal labeled SGNs were densely organized and coiled along the length of the cochlear duct at P0, X-Gal staining for *Isl1-lacZ* expression in the inner ear whole mounts and sections showed that the *Isl1*-deficient SGNs formed clump and failed to distribute along the coiled cochlear duct (Fig. 1*E–G*). We also assessed VGNs that consist of superior vestibular ganglion (SVG) and inferior vestibular ganglion (IVG) cells. In contrast to the orderly and compact arrangement of SVG neurons observed in controls, SVG neurons in *Isl1CKO* mice showed a scattered and disorganized distribution (Fig. 1*E*,*H*). To further verify the developmental defects of SGNs and VGNs in *Isl1CKO* mice, we performed DiI-labeling to highlight the neurons and their processes. Consistent with X-Gal staining results, DiI-labeling revealed similar defects of SGNs and VGNs in *Isl1CKO* inner ear at P0 (Fig. 1*I–K*). While SGNs were regularly distributed along the cochlea in controls, the regular distribution pattern of SGNs was disrupted in *Isl1CKO* mice, and SGNs were found closer to the modiolus (Fig. 1*I*). Likewise, DiI-labeling showed that in *Isl1CKO* mice, the number of IVG and SVG neurons was dramatically decreased, and the fiber projection to the posterior crista was completely lost (Fig. 1*J*,*K*). Collectively, these results demonstrate that inactivation of *Isl1* disrupts the orderly arrangement of SGNs and VGNs and results in their dramatic loss.

Isl1 inactivation disrupts the differentiation of CVG neurons

To determine how *Isl1* inactivation leads to SGN defects, we analyzed the generation and differentiation of CVG neurons at various developmental stages using three well-characterized CVG markers, NEUROD1, POU4F1, and POU4F2 (Kim et al., 2001; Deng et al., 2014). In mice, CVG neurons originate from the otic placode at E9.5 and most CVG neurons are formed between E10.5 and E11.5 (Fritzsch et al., 1999). NEUROD1 is one of the earliest CVG markers (Kim et al., 2001; Deng et al., 2014), and its expression is downregulated in the central region where CVG neurons exit the cell cycle, start to differentiate and express POU4F2 (Davies, 2007; Deng et al., 2014). Compared with the expression patterns of NEUROD1, POU4F1, and POU4F2 in the controls, the $NEUROD1^-$ central region was not well defined at E10.5 (Fig. 2*A*), and no $POU4F2^+$ CVG cell was detected in *Isl1CKO* mice (arrow in Fig. 2*B*), implying that the differentiation of CVG neurons is affected at this stage. However, $POU4F1^+$ CVG cells showed no significant difference between *Isl1CKO* and control inner ears ($n = 6$) (Fig. 2*B*,*D*). Interestingly, the downregulation of NEUROD1 and the onset of POU4F2 expression were detected in a subset of CVG neurons in *Isl1CKO* mice at E11.5 (arrows in Fig. 2*C*,*D*), implying that *Isl1* inactivation leads to the delayed differentiation of CVG neurons. To further define the effect of *Isl1CKO* on the differentiation of CVG, we performed immunolabeling for ISL1 along with NEUROD1 labeling. Immunolabeling of ISL1 antibody detected both $ISL1^+$ proliferating CVG cells and $ISL1^+/ISL2^+$ postmitotic CVG

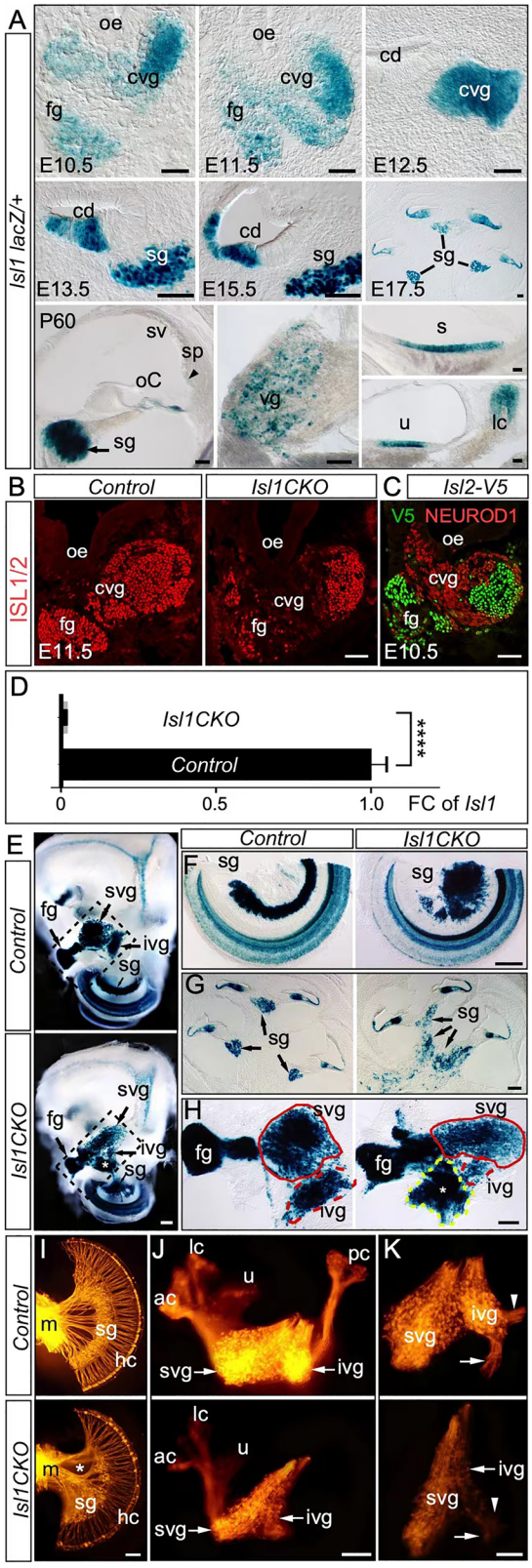

Figure 1. Inactivation of *Isl1* results in abnormal distribution and reduction of inner ear sensory neurons. ***A***, X-Gal staining of *Isl1*$^{lacZ/+}$ inner ears reveals the spatiotemporal expression pattern of *Isl1-lacZ* in developing sensory neurons. ***B***, ISL1/2 immunolabeling shows the ablation of ISL1 expression in *Isl1*-deficient CVG neurons at E11.5. Note that ISL1 expression remains in the facial ganglion and that the signals in the central CVG region likely show the expression of ISL2. ***C***, Co-labeling of *Isl2*-V5 knock-in mice with antibodies against V5 and NEUROD1 showing ISL2 expressing in the central CVG region. ***D***, Relative fold change of *Isl1* mRNA expression in E11.5 *Isl1CKO* inner ears by RT-PCR using primers in exons 2 and 3. ***E***, Whole mount X-Gal staining of the P0 inner ear shows that inactivation of *Isl1* disturbs the spatial distribution of inner ear sensory neurons. ***F,G***, X-Gal staining of the P0 cochlea whole mount (***F***) and sagittal section (***G***) reveal the altered distribution of SGNs in *Isl1CKO*. ***H***, Flat-mounts of the boxed area in ***E*** show the dramatic loss of inferior vestibular ganglion (ivg) cells in *Isl1CKO* mice. Asterisks in ***E*** and ***H*** mark ectopically located cells that do not appear to be part of the SGNs, inferior or superior vestibular ganglion in the *Isl1CKO* inner ear. ***I***, DiI labeling (P0) shows the morphological and projection defects of the spiral and vestibular ganglion neurons in *Isl1CKO* mice. Asterisks show the absence of SGNs in the hook region in *Isl1CKO* cochlea. ***J,K***, Flat-mount DiI labeling shows the defects of fiber projection and reduction of VGNs in *Isl1CKO* inner ear. Arrows indicate fiber projected to the saccule and arrowheads indicate fiber projected to the posterior crista. oe, otic epithelium; cvg, cochleovestibular ganglion; fg, facial ganglion; cd, cochlear duct; sg, spiral ganglion; vg, vestibular ganglion; s, saccule; u, utricle; oC, organ of Corti; svg, superior vestibular ganglion; ivg, inferior vestibular ganglion; m, modiolus; hc, hair cell; ac, anterior crista; lc, lateral crista; pc, posterior crista. Scale bars, 50 μm in (***A***); 100 μm in (***B,C,E–K***).

neurons in the controls (Fig. 2*E,F*). In comparison, the expression of ISL1 was absent and anti-ISL1 immunolabeling marked the ISL2^{+} postmitotic CVG neurons in *Isl1CKO*. Consistently, co-labeling with NEUROD1 and ISL1 antibodies revealed that the number of NEUROD1^{-}/ISL2^{+} differentiated CVG neurons in the central region was reduced in *Isl1CKO* compared to the controls at E10.5 and E11.5 (Fig. 2*E,F,K*), suggesting the disruption of CVG differentiation in *Isl1CKO*. We also labeled mitotic cells at S-phase with 5-bromo-2'-deoxyuridine (BrdU) and found that compared to the controls, the BrdU^{-} central CVG region was smaller in *Isl1CKO* at E10.5 (Fig. 2*G*), suggesting that CVG neurons fail to exit cell cycle on time in *Isl1CKO* mice. Taken together, these results indicate that *Isl1* is not required for the initial generation of CVG neurons and that *Isl1* inactivation disrupts the cell cycle exit and differentiation of CVG neurons.

Inactivation of *Isl1* affects migration and axon pathfinding of CVG neurons and leads to programmed cell death

During development, CVG neurons go through migration and axon pathfinding processes to position their cell bodies and to establish proper synaptic contacts with hair cells. We tested the role of *Isl1* in regulating the migration and axon pathfinding of developing CVG neurons at E14.5. While SGNs of the control mice were orderly distributed and extended their fibers to hair cells, SGNs of *Isl1CKO* mice were scattered and irregularly distributed, and areas devoid of fibers were frequently observed (Fig. 2*H*, asterisks), which was similarly observed at P0 (Fig. 1*I*). In addition, the fibers of VGNs extending to the anterior and posterior crista were dispersed and bifurcated in *Isl1CKO* mice (Fig. 1*J*), implying an axon pathfinding defect of *Isl1CKO* VGNs. Combined with X-Gal staining (Fig. 1*E–H*), these data suggested that *Isl1* could play a pivotal role in regulating the migration and axon pathfinding of CVG neurons.

To address how *Isl1* inactivation impacts the number of SGNs and VGNs, we investigated cell apoptosis in *Isl1CKO* CVG neurons using anti-CASP3 immunolabeling. At E11.5, there was no difference in CVG apoptosis between controls and *Isl1CKO* (Fig. 2*L*). At E12.5, apoptosis was significantly elevated in the CVG neurons of *Isl1CKO* (Fig. 2*L*). The peak of apoptosis of SGNs and VGNs appeared at E13.5 and lasted to at least E14.5 (Fig. 2*I,L*). Consistently, anti-POU4F2 immunolabeling of sections showed a significant loss of SGNs in *Isl1CKO* inner ears (Fig. 2*J*). These data indicate that *Isl1* is required for the survival of CVG neurons.

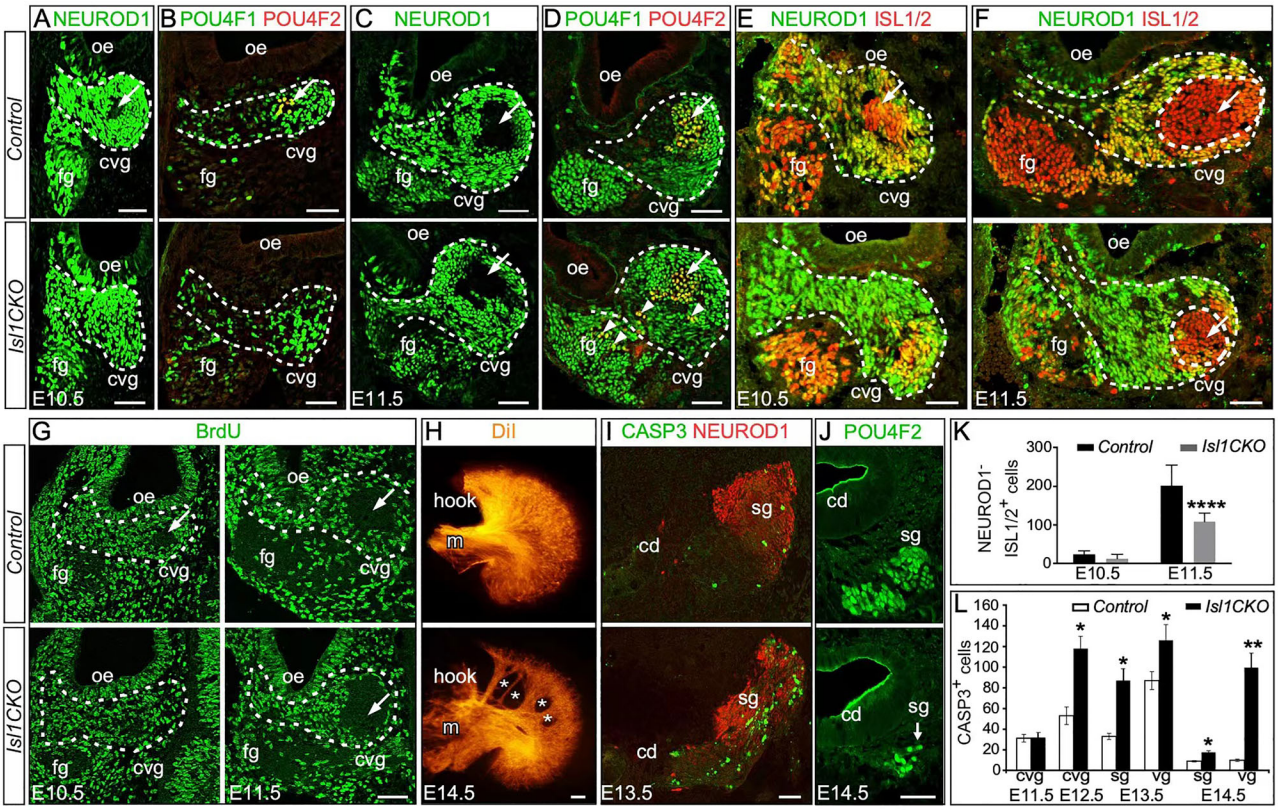

Figure 2. Inactivation of *Isl1* causes a delay in the differentiation and an increase in apoptosis of CVG neurons. ***A–D***, Immunolabeling of inner ear sections for NEUROD1, POU4F1 and POU4F2. Formation of NEUROD1$^-$/POU4F2$^+$ central CVG region is hardly seen in *Isl1CKO* at E10.5 (***A,B***) but is comparable to the control at E11.5 (***C,D***). Arrows indicate differentiated CVG neurons in central region. Arrowheads indicate POU4F2$^+$ differentiating CVG and FG neurons. Dashed boxes indicate CVG region. ***E,F***, NEUROD1 and ISL1/2 co-labeling of inner ear sections at E10.5 (***E***) and E11.5 (***F***) show the reduced ISL2$^+$ central CVG region (arrows) in *Isl1CKO* compared to the controls. ***G***, BrdU labeling of inner ear sections. At E10.5, a BrdU$^-$ central CVG region (arrows) is readily identified in the controls but not found in *Isl1CKO* at E10.5. No difference in cell proliferation is seen between control and *Isl1CKO* at E11.5. Dashed boxes indicate CVG region. ***H***, DiI-labeling of afferent projection to the basal turn of cochlea shows the reduction in fiber density (asterisks) in the *Isl1CKO* mice compared with the organized and dense fiber innervation in the control. ***I***, At E13.5, NEUROD1 and CASP3 immunostaining reveal increased cell death in the SGNs of the *Isl1CKO* mice compared with control. ***J***, At E14.5, POU4F2$^+$ SGNs (arrow) are significantly decreased in the *Isl1CKO* mice compared with control. ***K***, Quantitation of ISL1/2$^+$/NEUROD1$^-$ cells in the central region of CVGs at E10.5 and E11.5. Data are expressed as mean ± SEM ($n > 3$). ****$p < 0.001$. ***L***, Quantitation of CASP3$^+$ cells show that cell death is significantly increased in the CVG neurons of the *Isl1CKO* mice from E12.5. Data are expressed as mean ± SEM ($n = 6$). *$p < 0.05$; **$p < 0.01$. m, modiolus; cd, cochlear duct; sg, spiral ganglion; cvg, cochleovestibular ganglion; fg, facial ganglion; oe, otic epithelium. Scale bars, 50 µm in (***A–G,I,J***), 100 µm in (***H***).

ISL1 and POU4F1 interact directly to co-regulate the differentiation and survival of CVG neurons

Previously, studies have shown that ISL1 and POU4F TFs function in the same regulatory pathways to regulate neuronal differentiation (Pan et al., 2008; Dykes et al., 2011). We thus characterized the functional relationship of *Isl1* and *Pou4f1* in developing SGNs. We first examined SGNs in *Isl1CKO*, *Pou4f1KO*, and *Isl1/Pou4f1* double knock-out mice (*DKO*) at P0 using immunostaining with antibodies against SGN markers NEUN and CALRETININ. Compared to the control, the immunostaining revealed the reduction and disorganization of SGNs in the inner ear lacking either *Isl1* or *Pou4f1* and strikingly, the loss of almost all of the SGNs in the *DKO* inner ear (Fig. 3).

We further examined SGNs in *Isl1CKO*, *Pou4f1KO*, and *Isl1/Pou4f1 DKO* mice at E14.5 and P0 using DiI labeling. Compared with controls, disorganization and reduction in the number of the SGNs were readily seen in *Isl1CKO*, *Pou4f1KO*, and *DKO* inner ears at E14.5 (Fig. 4*A*). While DiI labeling showed the reduction of SGNs in *Isl1CKO* and *Pou4f1KO* mice, almost all of the SGNs were lost in the *DKO* inner ear at P0 (Fig. 4*B*). In addition, compared with the densely and orderly organized afferent fibers observed in controls, the overall fiber density was decreased in *Isl1CKO* or *Pou4f1KO* cochleae and only a very limited number of afferent fibers were detected in *DKO* mice at P0 (Fig. 4*B*). The arrangement of remaining fibers was also profoundly disturbed in *DKO* mice (Fig. 4*B*). The severe phenotype seen in *DKO* mice suggests that *Isl1* and *Pou4f1* might co-regulate the migration, axon pathfinding and survival of SGNs.

To understand the SGN defect seen in *DKO* mice, we examined the initial generation of CVG neurons by labeling of two early neuronal markers, NEUROD1 and SOX2, and a differentiated CVG marker, *Myt1* (Sun et al., 2022). At E10.5, the expression of NEUROD1 was detected in CVG neurons of the *Isl1CKO*, *Pou4f1KO*, and *DKO* mice, indicating that CVG neurons are generated and delaminated normally in these mutants (Fig. 4*C*). Consistently, in contrast to the controls, NEUROD1 downregulated central region was smaller in *Isl1CKO* mice. However, NEUROD1 was hardly downregulated in the central region of CVG neurons in *Pou4f1KO* and *DKO* mice at E10.5 (Fig. 4*C*). Similarly, co-labeling with anti-NEUROD1 antibody and *Myt1* RNAScope probe did not detect differentiated CVG neurons (NEUROD1$^-$/*Myt1*$^+$) in *Pou4f1KO* and *DKO* at E10.5 (Fig. 4*C*). Similar to NEUROD1 expression, SOX2 downregulation in CVG neurons was increasingly attenuated in an order of *control* < *Isl1CKO* < *Pou4f1KO* < *DKO* (Fig. 4*D*). Moreover, compared to *Pou4f1KO* and *Isl1CKO* mice at E11.5, compound mutation of

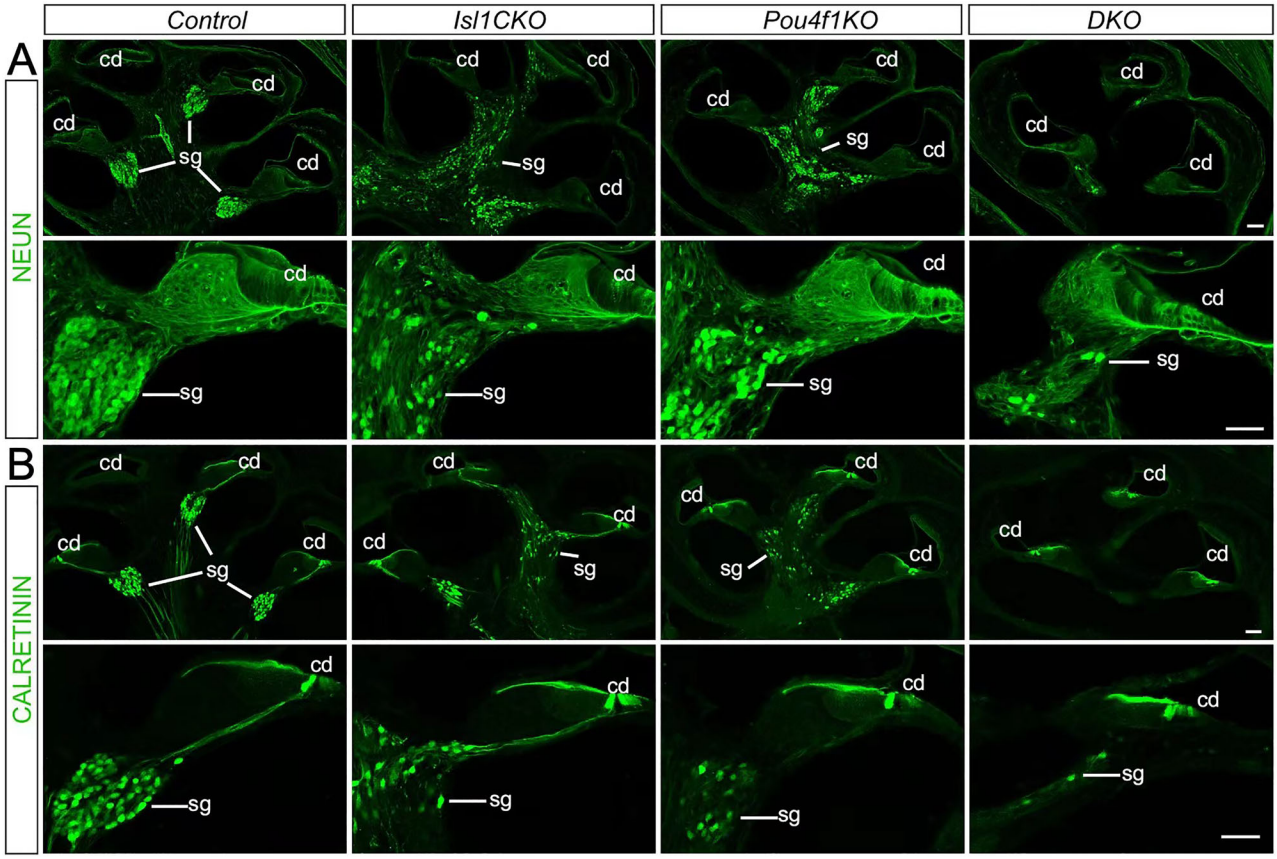

Figure 3. Targeted inactivation of *Isl1* and *Pou4f1* results in the reduction of spiral ganglion neurons at P0. Inner ear cryosections of the control, *Isl1CKO*, *Pou4f1KO* and *Isl1/Pou4f1 DKO* at P0 were immunolabeled with antibodies against NEUN (***A***) and CALRETININ (***B***), both makers of SGNs, showing a reduction of SGNs in the inner ears lacking either *Isl1* or *Pou4f1* and almost complete loss of SGNs in the inner ear deficient of both *Isl1* and *Pou4f1*. cd, cochlear duct; sg, spiral ganglion. Scale bar, 100 µm.

Isl1 and *Pou4f1* further blocked NEUROD1 downregulation (Fig. 4*E*). Consistently, we evaluated the effect of *DKO* on CVG apoptosis using anti-CASP3 immunolabeling at E13.5 and found that loss of *Isl1* significantly increased the number of $CASP3^{+}$ apoptotic SGNs while inactivation of *Pou4f1* had no significant effect (Fig. 4*F*). Intriguingly, compound mutation of *Isl1* and *Pou4f1* led to a greater loss of SGNs than that in *Isl1CKO* mice (Fig. 4*F*).

The more severe phenotypes observed in *DKO* mice along with the co-expression of ISL1 and POU4F1 in developing CVG neurons prompted us to test whether ISL1 directly interacts with POU4F1 during CVG development. We performed the proximity ligation assay (PLA), which enables the detection of direct protein-protein interaction in situ in cells and tissues (Fredriksson et al., 2002; Hegazy et al., 2020), to evaluate the relationship between ISL1 and POU4F1 in the CVG neurons. Compared to an absence of signals in controls without primary antibody or with antibody against either ISL1 or POU4F1 alone, addition of both anti-ISL1 and anti-POU4F1 antibodies revealed strong signals in the nuclei of CVG neurons at E10.5 (Fig. 4*G*), implying a direct interaction between ISL1 and POU4F1. Collectively, these data show that ISL1 and POU4F1 interact directly to regulate the differentiation and survival of CVG neurons.

Isl1 and *Pou4f1* epistatically regulate CVG-specific genes

To elucidate the GRN of *Isl1* and *Pou4f1* and to investigate how they regulate CVG development, we performed RNA-Seq analysis of the control, *Isl1CKO*, *Pou4f1KO*, and *DKO* CVG neurons at E11.5 when CVG defects are evident but CVG apoptosis has not started yet. We identified 761 downregulated genes and 445 upregulated genes (p adj <0.05, Log2FC > 2) in CVG neurons null for *Isl1* or *Pou4f1* or both (Fig. 5*A*). We noted that these differentially expressed genes (DEGs) were affected by the inactivation of *Isl1* or *Pou4f1* alone or both. We classified these DEGs into 3 subgroups and 8 clusters based on the genotypes for further overlapping analysis. The main group (cluster 1–4) consists of genes whose expression were altered in *DKO* CVG neurons, e.g., *Ntng2*, *Meis2*, *Eya1*, *Shh*, and *Sall3* (Fig. 5*B*). The other two groups (cluster 5–8) were mainly impacted by inactivation of either *Isl1* (e.g., *Gata3*, *Fgf10*, *Ntrk3*, and *Epha5* of cluster 5) or *Pou4f1* (e.g., *Pou4f2* and *Isl2* of cluster 7) (Fig. 5*B*). Importantly, many of these DEGs have known roles in CVG development (Schimmang et al., 1995; Fritzsch et al., 1998; Luo et al., 2013), indicating that *Isl1* and *Pou4f1* cooperatively as well as independently regulate genes associated with CVG differentiation.

Gene Ontology (GO) terms analysis showed that the DEGs positively regulated by both *Isl1* and *Pou4f1* were highly enriched in the biological processes of axonogenesis, axon guidance, neuron projection guidance and synapse organization (e.g., *Ntng2*, *Epha10*, *Sema3e*, *Ngfr*, *Shh*, and *Ntrk2*) (Fig. 5*C*). In addition, *Isl1* and *Pou4f1* independently activated genes commonly involved in biological processes of ear development, axonogenesis, and neuronal migration (e.g., *Gata3*, *Fgf10*, and *Ntrk3* of cluster 5 and *Pou4f2*, *Isl2*, and *Prrxl1* of cluster 7) (Fig. 5*D*). To confirm the RNA-Seq results, we performed qRT-PCR of 13

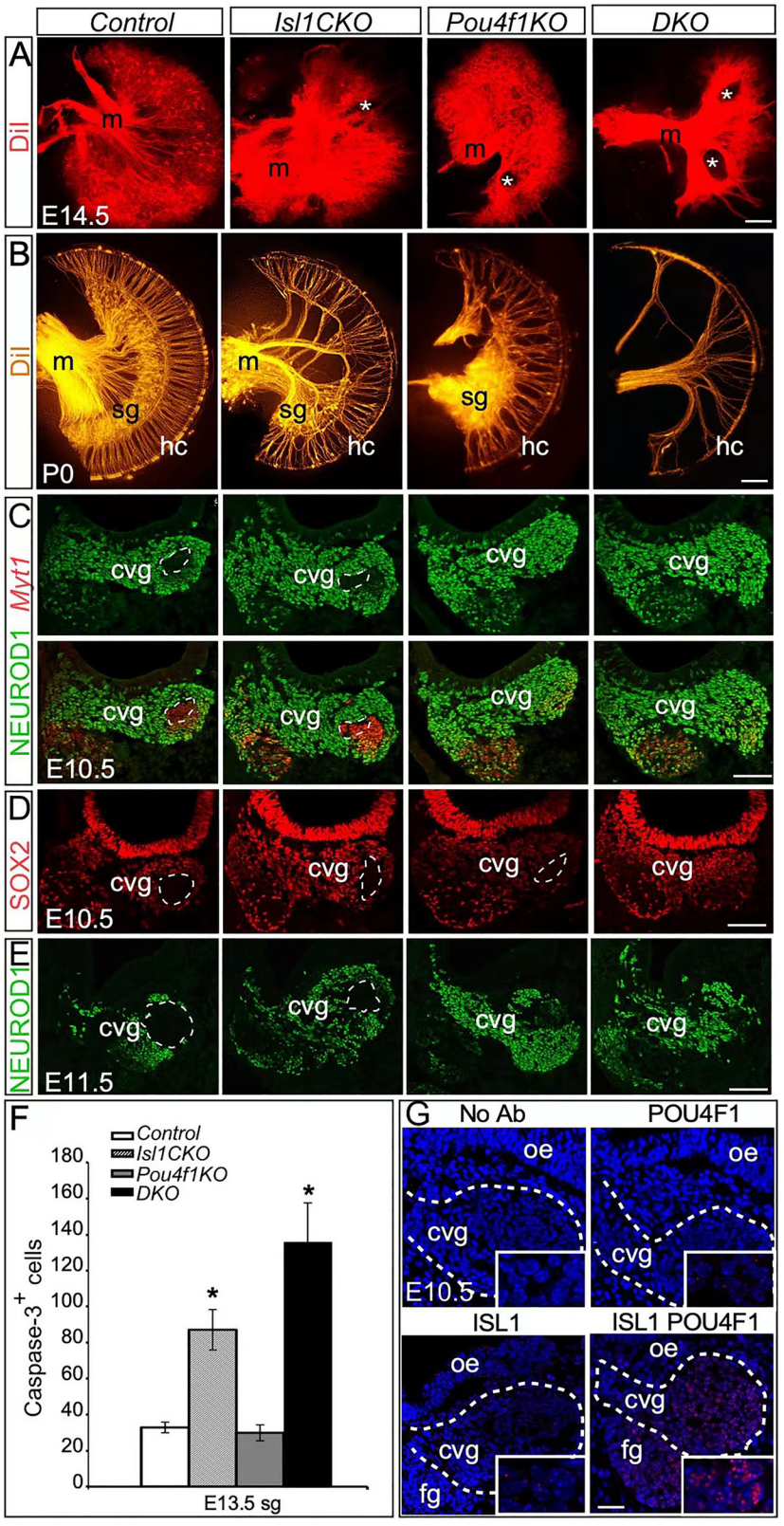

Figure 4. *Isl1* and *Pou4f1* cooperatively regulate the development of CVG and survival of SGNs. ***A,B***, DiI-labeling of SGN fibers shows the loss of SGNs and innervation defects in *Isl1CKO*, *Pou4f1KO*, and *DKO* mice at E14.5 (***A***) and P0 (***B***). ***C***, Combined immunolabeling of NEUROD1 and *Myt1* RNAScope ISH of the inner ear sections at E10.5. ***D,E***, Immunolabeling of the inner ear sections with antibodies against SOX2 at E10.5 (***D***) and NEUROD1 at E11.5 (***E***). ***F***, Quantitation of CASP3^{+} apoptotic cells of anti-CASP3 immunolabeled inner ear sections at E13.5. Data are expressed as mean ± SEM ($n = 6$). *$p < 0.05$. ***G***, Proximity Ligation Assay using no primary antibody, anti-ISL1, anti-POU4F1, and anti-ISL1/anti-POU4F1 antibodies at E10.5 CVG transverse sections. Dashed boxes indicate CVG region. m, modiolus; sg, spiral ganglion; hc, hair cell; oe, otic epithelium; cvg, cochleovestibular ganglion; fg, facial ganglion. Scale bars, 100 µm (***A–E***), 30 µm (***G***).

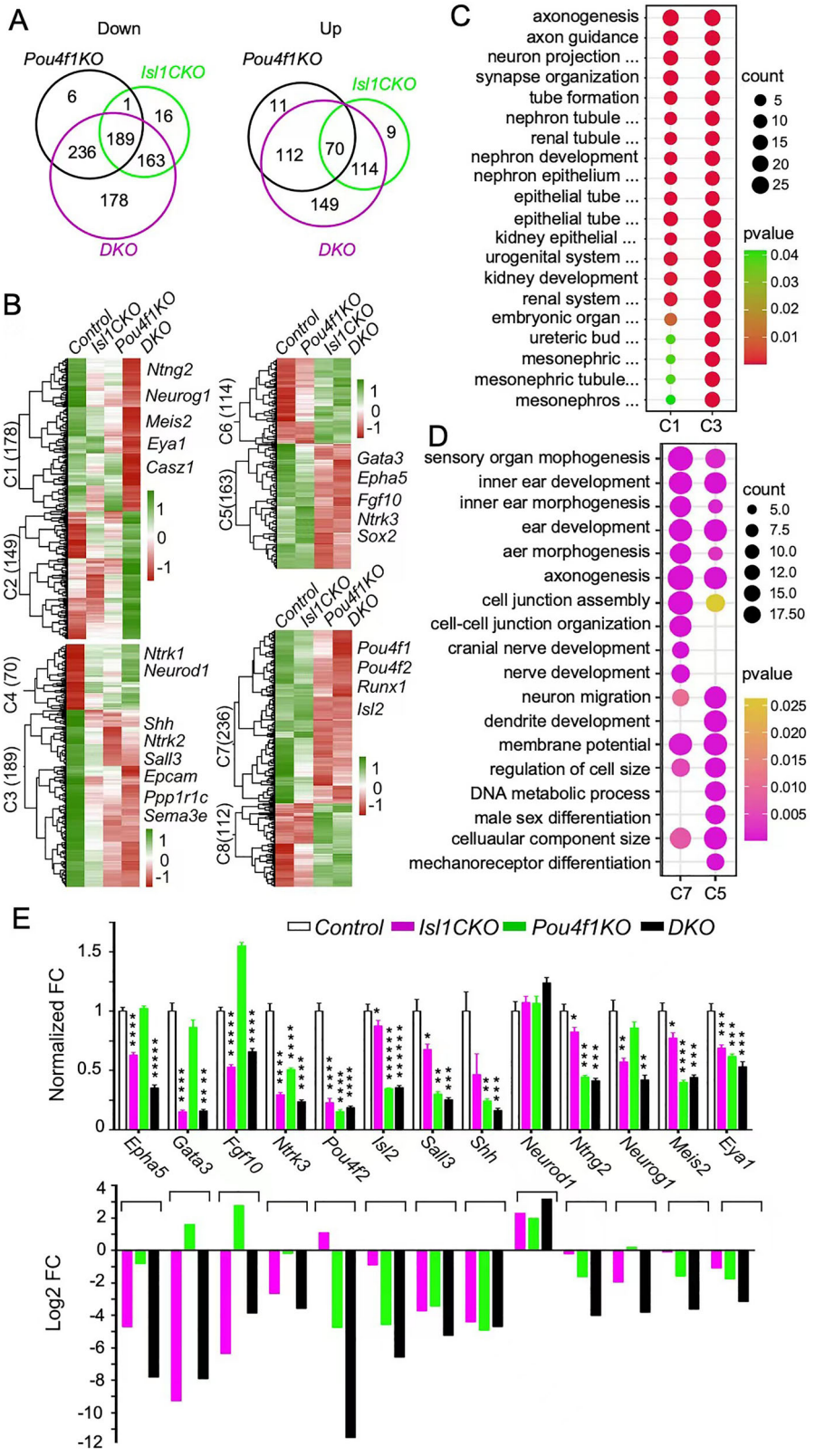

Figure 5. *Isl1* and *Pou4f1* epistatically or cooperatively regulate genes enriched in CVG neurons. ***A***, A Venn diagram indicating the overlap of DEGs down- or upregulated in *Pou4f1KO*, *Isl1CKO*, and *DKO* CVG neurons. ***B***, Clustered heatmaps of the 8 clusters of DEGs from ***A***. ***C***, Top 10 GO terms of cluster 1 and 3. Genes of cluster 3 are also enriched in the terms that cluster 1 is involved in. ***D***, Top 10 GO terms of cluster 5 and 7 show the common biological processes. ***E***, Changes in the expression of selected DEGs revealed by qRT-PCR and RNA-Seq analysis. qRT-PCR primers used were listed in Extended Data Table 5-1. Data are expressed as mean ± SEM ($n = 3$). *$p < 0.05$, **$p < 0.01$, ***$p < 0.001$ and so forth.

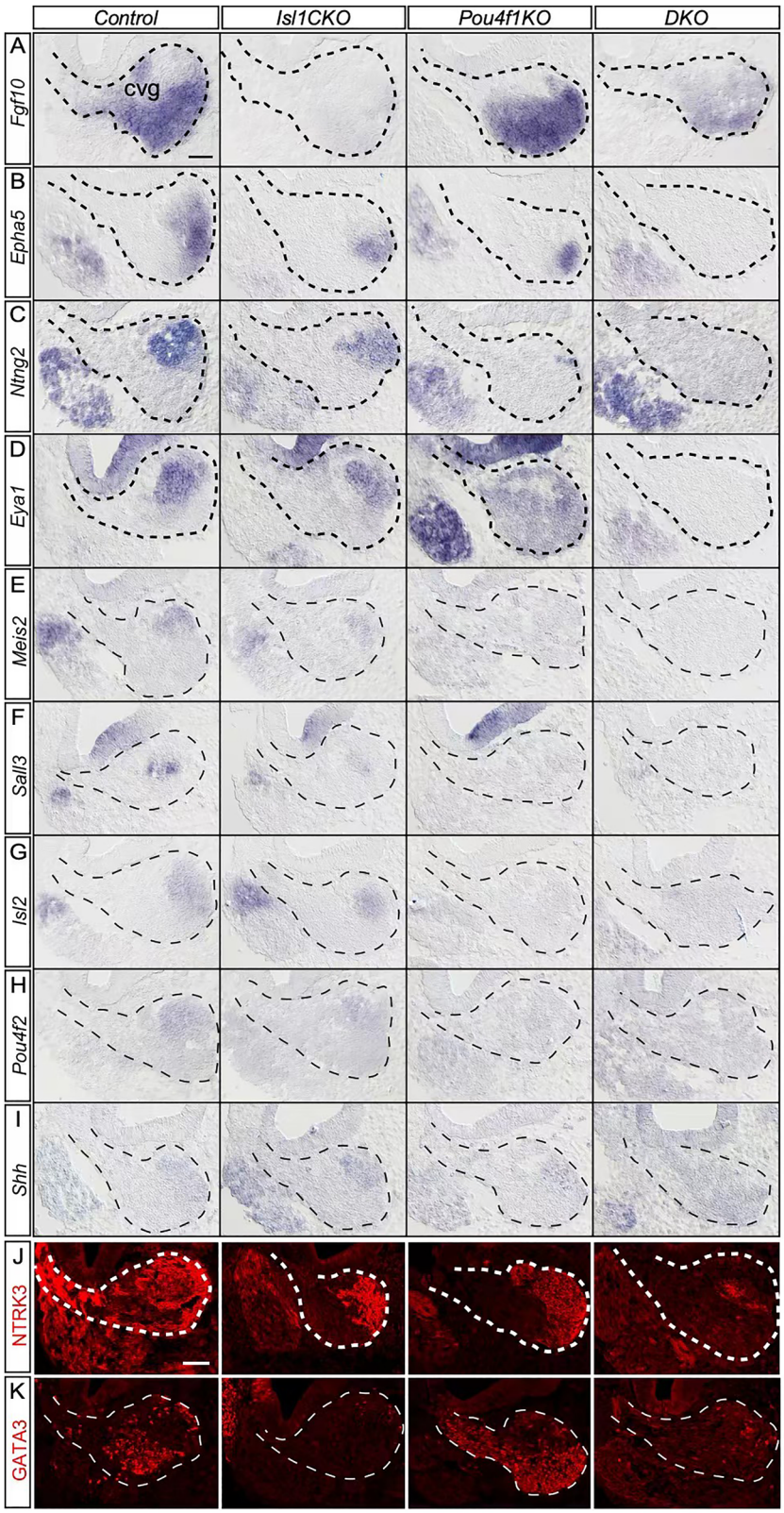

Figure 6. *Isl1* and *Pou4f1* regulate the expression of a common set as well as unique sets of CVG-specific genes. Confirmation of gene expression changes in CVG neurons by ISH and immunolabeling of inner ear cryosections of control, *Isl1CKO*, *Pou4f1KO* and *DKO* mice at E11.5. (***A***) *Fgf10*. (***B***) *Epha5*. (***C***) *Ntng2*. (***D***) *Eya1*. (***E***) *Meis2*. (***F***) *Sall3*. (***G***) *Isl2*. (***H***) *Pou4f2*. (***I***) *Shh*. (***J***) NTRK3. (***K***) GATA3. Dashed lines indicate CVG regions. Scale bars, 100 µm.

selected genes using control and mutant CVG neurons and normalized the expression levels to an internal control, *Actb*. Consistent with the RNA-Seq data, we noted that *Epha5*, *Gata3*, and *Fgf10* were down regulated in *Isl1CKO* and *DKO*, *Isl2* and *Pou4f2* downregulation was more severe in *Pou4f1KO* than in *Isl1CKO*, and *Sall3*, *Ntng2*, *Meis2*, and *Eya1* were

significantly downregulated in all three mutants (Fig. 5*E*). We further confirmed the changes in the expression of 11 genes mentioned above by in situ hybridization or immunolabeling in E11.5 CVG neurons. While all genes were dramatically downregulated in *DKO*, the downregulation of *Fgf10* and *Gata3* were largely caused by *Isl1* inactivation and conversely, *Isl2* and *Pou4f2* downregulation could be attributed mostly to the loss of *Pou4f1* (Fig. 6). Thus, *Isl1* and *Pou4f1* co-regulate a common set of genes and also act independently to control separate groups of genes essential for CVG development.

ISL1 and POU4F1 directly bind to the regulatory elements in DEGs

To determine how *Isl1* and *Pou4f1* regulate the DEGs identified by RNA-Seq analysis, we identified genomic regions occupied by ISL1 and POU4F1 using the CUT&Tag approach (Kaya-Okur et al., 2020), which is developed from ChIP-Seq and CUT&RUN (Skene and Henikoff, 2017) for its high specificity with a low number of cells, and compared these regions to those bound by H3K4me3 and H3K27ac or by H3K27me3, which mark active or silenced chromatin regions, respectively. Data from duplicate experiments of each protein were combined and peaks were called against IgG controls. The locations of ISL1- and POU4F1-bound peaks showed a significant enrichment at the proximity of transcriptional start site (TSS) (Fig. 7*A*), suggesting their roles in initiating transcription. Genomic feature annotation showed more than half of ISL1 (78.5%) and POU4F1 (80%) peaks were distal, intergenic, and intronic, which is similar with those of H3K27ac (62.4%), but different from those of H3K27me3 (36.5%) and H3K4me3 (7.7%). The majority of H3K27me3 (53%) and H3K4me3 (91.1%) bindings are enriched in promoter region, which is consistent with their known roles (Fig. 7*B*). These results suggest that ISL1 and POU4F1 could activate the transcription potentially via engaging in the promoter-enhancer contacts.

To identify the genes directly regulated by ISL1 and POU4F1, we first filtered the peak regions for predicted binding sites by Bedtools intersect and identified a total of 1,459 ISL1-bound and 5,446 POU4F1-bound genes (Fig. 7*C*). By integrating these genes with the DEGs identified by RNA-Seq analysis, we obtained 103 downregulated and 30 upregulated genes co-bound by ISL1 and POU4F1, 48 ISL1-bound and 220 POU4F1-bound downregulated genes and 24 ISL1-bound and 132 POU4F1-bound upregulated genes (Fig. 7*C*). GO term enrichment analysis showed that ISL1 and POU4F1 targeting genes were often related to neuronal system, nervous system development and axon guidance (Fig. 7*D*).

The CUT&Tag peaks of ISL1 and POU4F1 were further examined by intersecting with snATAC-Seq peaks identified from SGNs and VGNs at E12.5. The snATAC-Seq peaks identified from a cluster of prosensory cells (Ps cells) were plotted as non-neuronal controls. The representative Integrative Genomics Viewer (IGV) genome track snapshots showed the binding sites of ISL1 or POU4F1 or both at the verified downregulated genes: a highly active distal enhancer in *Eya1* with a specificity in SGNs and VGNs and with H3K27ac-deposition was occupied by both ISL1 and POU4F1 (Fig. 7*E*); two highly active distal enhancers in *Ntng2* more dynamic in SGNs and VGNs and with H3K27ac-deposition were bound by ISL1 only (Fig. 7*E*); and a distal enhancer and an intronic enhancer with H3K27ac-deposition in *Ntrk3* were bound by ISL1 and POU4F1, respectively (Fig. 7*F*). We also identified quiescent regions such as the ISL1-bound *Epha5* promoter region and an ISL1-bound *Fgf10* promoter region with H3K27ac-, H3K27me3-, and H3K4me3-deposition. In addition, a distal enhancer with H3K27ac and H3K27me3 deposition in *Fgf10* was bound by ISL1 only (Fig. 7*G*). In *Pou4f2*, we found a POU4F1-bound biovalent promoter region with H3K4me3- and H3K27me3-deposition and a biovalent distal enhancer co-bound by ISL1 and POU4F1 (Fig. 7*G*). These two regions in *Pou4f2* have been previously reported to regulate the expression of *Pou4f2* in the retina (Ge et al., 2023). Furthermore, we found the occupancy of ISL1 and POU4F1 in other genes associated with axon guidance. For instance, *Sema3e* was bound by ISL1 at a neuron-specific distal enhancer (Fig. 7*H*), *Gap43* was co-bound by ISL1 and POU4F1 at a distal, an intronic, and a downstream highly active enhancers (Fig. 7*I*), and *Nrcam*, a gene expressed in SGNs and required for the innervation between SGNs and hair cells (Harley et al., 2018), was co-bound by ISL1 and POU4F1 at two intronic enhancers (Fig. 7*J*). In addition, *Ppp1r1c* and *Runx1*, two DEGs previously identified in *DKO* DRG neurons (Dykes et al., 2011), showed different patterns of ISL1 and POU4F1 occupancy that in *Ppp1r1c*, ISL1 and POU4F1 co-bind to an exonic and downstream enhancer (Fig. 7*K*), whereas ISL1 and POU4F1 individually bind to two distal enhancers in *Runx1* (Fig. 7*L*). Thus, these discoveries imply that ISL1 and POU4F1 could regulate the axon guidance and survival of the CVG neurons by shaping the epigenetic landscape of associated genes through binding to the active promoters or enhancers.

Enhancers bound by ISL1 and POU4F1 are functionally important in CVG neurons

As a first step to gain further insight into the mechanisms of ISL1 and POU4F1 function and to validate the biological significance of these *cis*-regulatory elements (CREs) in vivo, we used genome editing by CRISPR/Cas9 approach to delete selected CREs in mice and analyzed the effects on gene expression in homozygous deletion mutants by in situ hybridization. The expression of the neuron-enriched gene *Fgf10* is greatly downregulated in *Isl1CKO* (Figs. 5*E*, 6*A*), and two adjacent active CREs of *Fgf10* were bound by ISL1 (Fig. 7*G*). We designed two single-guide RNA (sgRNAs) to delete the 965 bp enhancer of *Fgf10* (Chr13: 118711166–118712131) (Figs. 7*G*, 8*A*,*B*) and found that the deletion of this *Fgf10* enhancer led to a significant reduction in *Fgf10* expression in CVG neurons at E11.5 (Fig. 8*C*), strongly arguing for its biological function in regulating *Fgf10* expression. Similarly, the downregulation of *Ntng2* in *DKO* mice (Figs. 5*E*, 6*C*) and occupancy of ISL1 at its two distal enhancers (Fig. 7*E*) prompted us to test their functional significance in vivo, too. We used two pairs of sgRNAs to remove the two distal enhancers containing multiple ISL1 binding sites predicted from JASPAR database, 805 bp at Chr2: 29272157–29272961 or ~24 kb upstream of the TSS and 1,563 bp at Chr2: 29285119–29286682 or ~35 kb upstream of the TSS (Fig. 8*A*,*B*). In addition, the ~35 kb *Ntng2* enhancer contains two predicted POU4F1 binding sites (Fig. 8*B*). Deletion of the ~24 kb upstream enhancer notably reduced the expression of *Ntng2* while the deletion of the ~35 kb upstream enhancer also resulted in, though to a lesser extent, a decrease in *Ntng2* expression (Fig. 8*C*). These findings further show that ISL1 and POU4F1 function epistatically as well as independently to regulate the CVG differentiation program.

Discussion

It is well established that ISL1 and POU4Fs are co-expressed in developing RGCs and sensory neurons of DRG and TG and

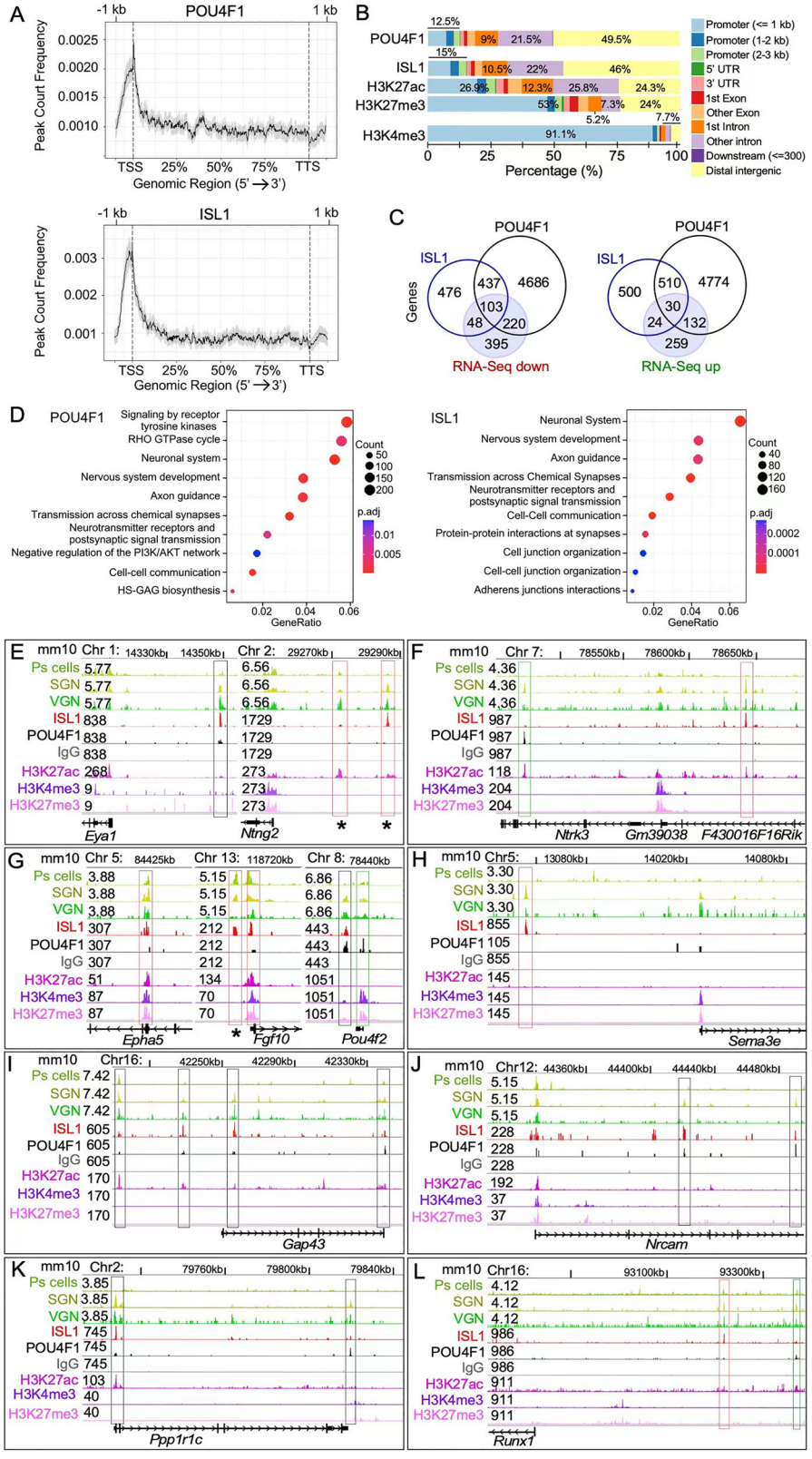

Figure 7. Epistatic and combinatorial regulation of CVG-specific genes by ISL1 and POU4F1 at E11.5. ***A***, Genomic distribution of POU4F1-bound (top) and ISL1-bound (bottom) peaks relative to the distance from transcriptional start site (TSS). TTS indicates the transcriptional termination site. ***B***, Genomic annotation of peaks identified by CUT&Tag analysis using antibodies against POU4F1, ISL1, H3K27ac, H3K27me3, and H3K4me3. ***C***, A Venn diagram showing the overlaps of DEGs identified by RNA-Seq and genes found by CUT&Tag analysis. 103 downregulated and 30 upregulated genes are ISL1 and POU4F1 co-bound. ***D***, Biological processes of POU4F1-bound (left) and ISL1-bound (right) genes are often related to neuronal system, nervous system development and axon guidance. ***E–L***, Integrative Genomics Viewer (IGV) track visualization of peaks identified by snATAC-Seq of prosensory cells, SGNs and VGNs, and CUT&Tag analysis using antibodies against POU4F1, ISL1, H3K27ac, H3K27me3, and H3K4me3. Colored boxes mark the genomic regions co-bound by ISL1 and POU4F1 (black boxes) or bound by just ISL1 (red boxes) or POU4F1 (green boxes). *Y*-axis value of each track indicates track height. The direction of transcription is shown by arrows. Asterisks indicate the peaks selected for functional tests in vivo.

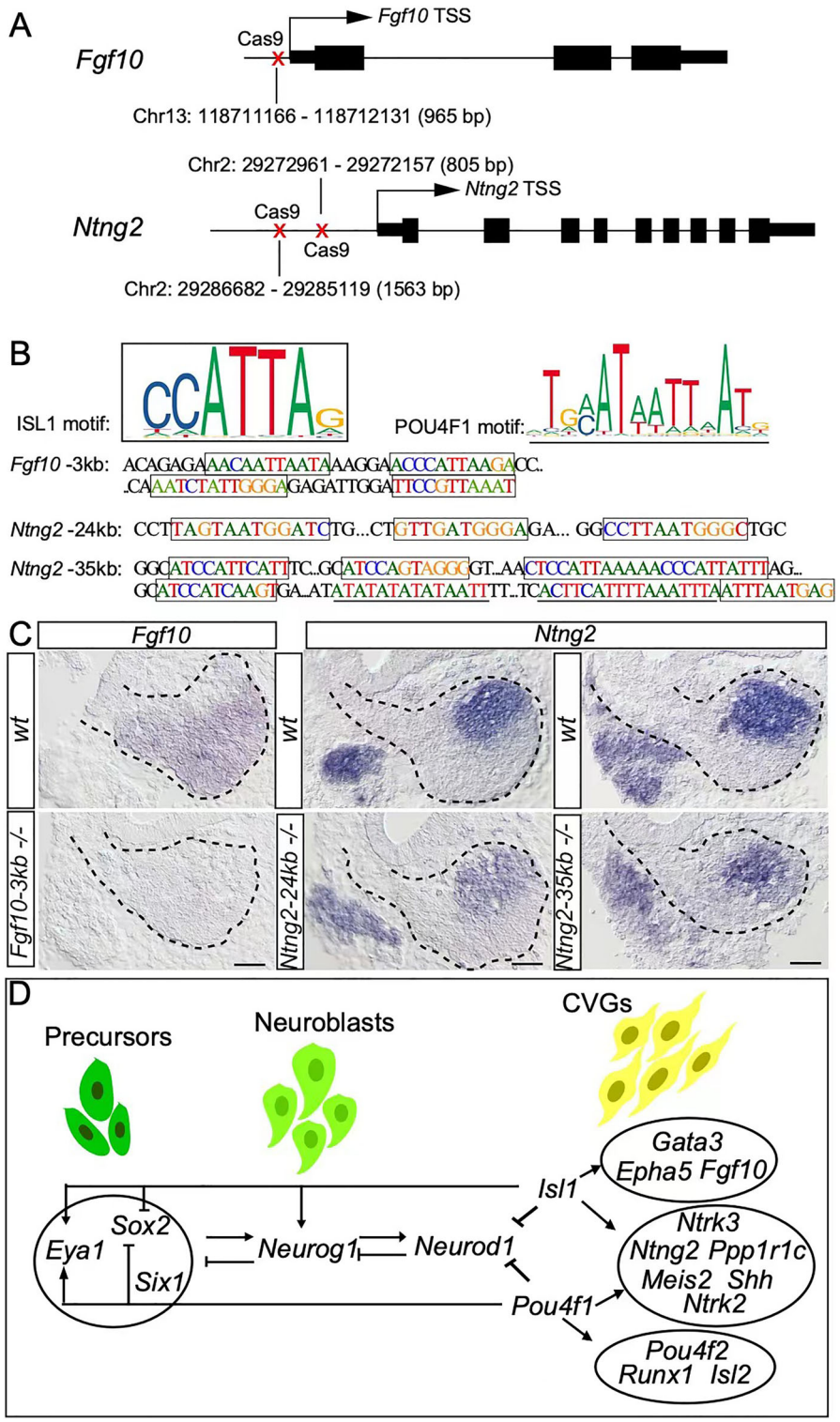

Figure 8. Deletions of ISL1-bound enhancers attenuate the expression of *Fgf10* and *Ntng2*. ***A***, Deletion strategies of ISL1-bound peaks in *Fgf10* and *Ntng2* using two Cas9 sgRNAs to flank each peak. sgRNAs and PCR genotyping primers used for enhancer deletions by CRISPR/Cas9 were listed in Extended Data Table 8-1. ***B***, Top panels are predicted ISL1 and POU4F1 motifs from JASPAR database. Lower panels show ISL1 and POU4F1 motifs in selected peaks. ***C***, ISH showing the downregulation of genes in CVG neurons of enhancer deletion mutants at E10.5. Dashes indicate the CVG region. cvg, cochleovestibular ganglion. Scale bar, 100 µm. ***D***, A graphic conclusion of the roles of *Isl1* and *Pou4f1* in the gene regulatory network during CVG differentiation.

regulate their development (Mu et al., 2008; Pan et al., 2008; Sun et al., 2008; Dykes et al., 2011). During RGC development, *Pou4f2*, which is expressed before *Pou4f1* and is required for activating *Pou4f1* expression, has a stronger effect than *Pou4f1* on RGC differentiation and the expression of RGC-specific genes (Gan et al., 1996; Pan et al., 2008). *Pou4f2* and *Isl1* function in the same genetic pathway to co-regulate RGC development. While knock-out of either gene results in a partial loss of RGCs, *Isl1/Pou4f2* DKO leads to the loss of nearly all RGCs (Pan et al., 2008). In TG and DRG neurons, the regulatory

relationship of *Pou4f1* and *Pou4f2* is reversed compared to that in RGCs, where *Pou4f1* is expressed before *Pou4f2* and is required for *Pou4f2* expression. Similarly, in *Pou4f1/Isl1* DKO mice, the initial formation of TG and DRG is not affected but DRG neurons are displaced, and their peripheral projections are disrupted (Dykes et al., 2011). In our current study, we found that *Isl1* controls the differentiation of SGNs and is required for their maintenance, axon pathfinding and migration. Without *Isl1*, a majority of SGNs fail to settle along the length of the cochlear duct and to extend neural fibers to hair cells, and a significant number of SGNs undergo apoptosis. These phenotypes are similar to those reported in a recent study (Filova et al., 2022) and further demonstrate the critical role of *Isl1* in SGN development. Moreover, *Pou4f1KO* leads to disorganization and reduction in SGNs though to a lesser extent than *Isl1CKO*, and *Pou4f1/Isl1* DKO severely disrupts SGN differentiation and results in a nearly complete loss of SGNs. Thus, our study uncovers a remarkable similarity of the role of *Pou4f1* and *Isl1* in developing SGNs and sensory neurons of TG and DRG, arguing for a conserved functional mechanism of *Isl1* and *Pou4fs* in both developing central and peripheral nervous systems.

The hallmarks of *Pou4f1/Isl1* DKO defects are the delayed cell cycle exit of CVG neurons, the disorganization and reduction in SGNs and neural fibers, and SGN death. As TFs, ISL1 and POU4F1 could promote cell cycle exit and neuronal differentiation by repressing neurogenic genes and activating genes essential for axon pathfinding and migration. Previous studies have shown that both *Isl1* and *Pou4f1* repress neurogenic bHLH genes of the *Neurog* and *Neurod* classes, e.g., *Neurod1*, *Neurod4*, and *Neurog1* in DRG and TG (Eng et al., 2007; Lanier et al., 2007; Dykes et al., 2011). Interestingly, we found that *Isl1* and *Pou4f1* co-repress *Neurod1* expression in CVG neurons (Fig. 4), providing an insight into how *Isl1* and *Pou4f1* regulate neurogenesis and cell cycle exit. Intriguingly, the SGN defects observed in the *DKO* mutants show some similarity to the phenotypic defects observed in *Neurod1*-null mice, in which approximately 90% of CVG neurons were lost (Kim et al., 2001). However, unlike *Neurod1*-null mice, *Isl1* and *Pou4f1* DKO do not affect the initial generation and delamination of CVG neurons, suggesting different roles of *Neurod1* in CVG neurogenesis and of *Isl1* and *Pou4f1* in CVG differentiation. Our previous study demonstrates a sequential expression order of NEUROD1 > ISL1 > POU4F1 > POU4F2 during the inner ear neurogenesis and shows that ISL1 expression in CVG neuron is downregulated in *Neurod1*-null mice but is not affected in *Pou4f1KO* CVG neuron (Deng et al., 2014). Here, we further show that *Isl1CKO* does not affect the expression of *Pou4f1* or the onset of *Neurod1* expression (Fig. 2*A–D*). These results suggest that *Isl1* and *Pou4f1* act in parallel and immediately downstream of *Neurod1* in a regulatory hierarchy of NEUROD1 > ISL1⇔POU4F1 to drive the differentiation of CVG neurons into SGNs.

To understand how ISL1 and POU4F1 regulate the differentiation, migration and axonogenesis of SGNs, we found through expression analysis that *Isl1/Pou4f1* DKO results in the downregulation of neurotrophin receptor genes (*Ntrk2* and *Ntrk3*) and RUNX gene (*Runx1*) (Figs. 5, 6), consistent with the finding that *Isl1* and *Pou4f1* positively regulate the expression of *Ntrk* and *Runx* in DRG and TG (Eng et al., 2007; Lanier et al., 2007; Sun et al., 2008). Additionally, *Ntng2* plays an essential role in axon guidance and homozygous missense mutation of *NTNG2* leads to developmental delay globally and other neurodevelopmental disorders in humans (Dias et al., 2019). Inactivation of *Isl1* or *Pou4f1* or both leads to the downregulation of *Ntng2* (Figs. 5, 6), which might contribute to defective SGN axonal processes observed in these mutant mice. Moreover, we discover that *Isl1* and *Pou4f1* activate *Eya1*, a pioneer gene upstream of *Neurog1* and essential for the survival of placodally delaminated sensory neurons (Zou et al., 2004). Interestingly, interaction between *Eya1* and *Six1* also plays a role in determining the neuronal fate and subtype identities of early auditory neurons (Zou et al., 2004; Ahmed et al., 2012). The downregulation of *Eya1* is first seen in the central CVG region in *Isl1/Pou4f1* DKO mice (Fig. 6*D*), suggesting *Eya1*'s late role downstream of *Isl1* and *Pou4f1* in the differentiation of postmitotic CVG neurons. Besides their many shared downstream target genes, *Isl1* and *Pou4f1* each regulate unique sets of genes. *Isl1* is largely responsible for the activation of *Fgf10* and *Gata3*, while *Isl2* and *Pou4f2* expression mostly rely on *Pou4f1* (Fig. 6). These data show that *Isl1* and *Pou4f1* epistatically regulate many of their target genes as well as play the predominant or exclusive role in regulating other unique sets of genes during CVG development.

In addition to its expression in early CVG neurons starting at E9.5 (Fedtsova and Turner, 1995), *Pou4f1* expression is found to be restricted in type I SGNs later (Shrestha et al., 2018; Sherrill et al., 2019; Petitpre et al., 2022). On the other hand, *Isl1* expression persists in both SGNs and VGNs. Many of the downstream DEGs found in this study are neuronal subtype-featured genes, for example, *Meis2*, *Gata3*, *Runx1*, *Epha5*, *Ntrk2*, *Ntrk3*, and *Casz1* (Shrestha et al., 2018; Petitpre et al., 2022). Considering their function of subtype specification in other system or species, potential roles of *Isl1* and *Pou4f1* in regulating the specification of auditory neuronal subtypes will be of great interest for future studies.

In our genome-wide search for the downstream effector genes directly regulated by *Isl1* and *Pou4f1*, we combined CUT&Tag and snATAC-Seq analyses to obtain the location and identity of ISL1 and POU4F1 binding sites at the downstream genes. These elements consist of promoters and active enhancers. Interestingly, we found that ISL1 and POU4F1 could co-regulate gene expression through binding to the same or different sites. The majority of ISL1 and POU4F1 binding sites are distal and intronic enhancers, suggesting their transactivating function through these enhancers (Fig. 7). It is known that the promoter-enhancer contacts orchestrate the genome-wide gene transcription (van Arensbergen et al., 2014); ISL1 and POU4F1 might regulate the cross-talking between promoters and enhancers by binding to these enhancers and bringing them together with promoters. Previous study in *Caenorhabditis elegans* reports that *unc-86* (a *Pou4f1* ortholog) and *mec-3* (an *Isl1* ortholog) form an UNC-86/MEC-3 heterodimer to bind to the promoters of *mec-4* and *mec-7* (Duggan et al., 1998). The co-expression of ISL1 and POU4F1 in developing CVG neurons and their epistatic interaction on their many target genes suggest that ISL1 and POU4F1 could form a heterodimer in CVG neurons. Indeed, our PLA assay provides the first in vivo evidence of the direct interaction between ISL1 and POU4Fs in the developing CVG neurons (Fig. 4*G*) and further suggests similar interactions between ISL1 and POU4Fs in other neurons.

Using CRISPR/Cas9 approach to delete enhancers bound by ISL1 and POU4F1, we found that the deletion of *Ntng2* enhancers shows different degree of effects on its expression in CVG neurons, and these effects are less severe than those observed in CVG null for *Is11* or *Pou4f1* or both, suggesting other factors or multiple regions are involved in these transcription processes. It is also possible that the interaction between ISL1 and POU4Fs could be far more complex than ISL1-POU4F dimer, such that

they might be involved in "transcription factory" for co-regulated subgroup of genes to share regulatory factors in a large subnuclear transcription structure within the nucleus (Edelman and Fraser, 2012). Future studies are needed to gain a further insight into the mechanism of ISL1 and POU4F1 in regulating CVG differentiation by fully characterizing ISL1 and POU4F1 binding sites and their functional significance.

Taken together, we have uncovered the essential role of ISL1 in the development of CVG neurons and SGNs. More importantly, we have revealed the novel direct interaction of ISL1 and POU4F1 and have identified the GRN of ISL1 and POU4F1 during the development of auditory neurons using a combined approach of genetic, protein-protein interaction, and multiomic methods. Our studies establish the role of *Isl1* and *Pou4f1* in developing CVG and define the diverse relationship among *Isl1*, *Pou4f1* and their target genes (Fig. 8*D*). Importantly, our findings shed light into the general principle of ISL1 and POU4Fs function in the development of various nervous systems.

References

Ahmed M, Xu J, Xu P-X (2012) EYA1 and SIX1 drive the neuronal developmental program in cooperation with the SWI/SNF chromatin-remodeling complex and SOX2 in the mammalian inner ear. Development 139:1965–1977.

Appler JM, Goodrich LV (2011) Connecting the ear to the brain: molecular mechanisms of auditory circuit assembly. Prog Neurobiol 93:488–508.

Chang W, Lin Z, Kulessa H, Hebert J, Hogan BL, Wu DK (2008) Bmp4 is essential for the formation of the vestibular apparatus that detects angular head movements. PLoS Genet 4:e1000050.

Concordet JP, Haeussler M (2018) CRISPOR: intuitive guide selection for CRISPR/Cas9 genome editing experiments and screens. Nucleic Acids Res 46:W242–W245.

Davies D (2007) Temporal and spatial regulation of alpha6 integrin expression during the development of the cochlear-vestibular ganglion. J Comp Neurol 502:673–682.

Deng M, Pan L, Xie X, Gan L (2010) Requirement for Lmo4 in the vestibular morphogenesis of mouse inner ear. Dev Biol 338:38–49.

Deng M, Yang H, Xie X, Liang G, Gan L (2014) Comparative expression analysis of POU4F1, POU4F2 and ISL1 in developing mouse cochleovestibular ganglion neurons. Gene Expr Patterns 15:31–37.

Dias CM, et al. (2019) Homozygous missense variants in NTNG2, encoding a presynaptic netrin-G2 adhesion protein, lead to a distinct neurodevelopmental disorder. Am J Hum Genet 105:1048–1056.

Duggan A, Ma C, Chalfie M (1998) Regulation of touch receptor differentiation by the *Caenorhabditis elegans* mec-3 and unc-86 genes. Development 125:4107–4119.

Dykes IM, Tempest L, Lee SI, Turner EE (2011) Brn3a and Islet1 act epistatically to regulate the gene expression program of sensory differentiation. J Neurosci 31:9789–9799.

Edelman LB, Fraser P (2012) Transcription factories: genetic programming in three dimensions. Curr Opin Genet Dev 22:110–114.

Elshatory Y, Everhart D, Deng M, Xie X, Barlow RB, Gan L (2007) Islet-1 controls the differentiation of retinal bipolar and cholinergic amacrine cells. J Neurosci 27:12707–12720.

Eng SR, Dykes IM, Lanier J, Fedtsova N, Turner EE (2007) POU-domain factor Brn3a regulates both distinct and common programs of gene expression in the spinal and trigeminal sensory ganglia. Neural Dev 2:3.

Fedtsova NG, Turner EE (1995) Brn-3.0 expression identifies early post-mitotic CNS neurons and sensory neural precursors. Mech Dev 53:291–304.

Fettiplace R, Hackney CM (2006) The sensory and motor roles of auditory hair cells. Nat Rev Neurosci 7:19–29.

Filova I, et al. (2022) ISL1 is necessary for auditory neuron development and contributes toward tonotopic organization. Proc Natl Acad Sci U S A 119.

Fredriksson S, Gullberg M, Jarvius J, Olsson C, Pietras K, Gustafsdottir SM, Ostman A, Landegren U (2002) Protein detection using proximity-dependent DNA ligation assays. Nat Biotechnol 20:473–477.

Fritzsch B (2003) Development of inner ear afferent connections: forming primary neurons and connecting them to the developing sensory epithelia. Brain Res Bull 60:423–433.

Fritzsch B, Barbacid M, Silos-Santiago I (1998) The combined effects of trkB and trkC mutations on the innervation of the inner ear. Int J Dev Neurosci 16:493–505.

Fritzsch B, Muirhead KA, Feng F, Gray BD, Ohlsson-Wilhelm BM (2005) Diffusion and imaging properties of three new lipophilic tracers, NeuroVue maroon, NeuroVue Red and NeuroVue green and their use for double and triple labeling of neuronal profile. Brain Res Bull 66:249–258.

Fritzsch B, Pirvola U, Ylikoski J (1999) Making and breaking the innervation of the ear: neurotrophic support during ear development and its clinical implications. Cell Tissue Res 295:369–382.

Gan L, Xiang M, Zhou L, Wagner DS, Klein WH, Nathans J (1996) POU domain factor Brn-3b is required for the development of a large set of retinal ganglion cells. Proc Natl Acad Sci U S A 93:3920–3925.

Gan L, Wang SW, Huang Z, Klein WH (1999) POU domain factor Brn-3b is essential for retinal ganglion cell differentiation and survival but not for initial cell fate specification. Dev Biol 210:469–480.

Ge Y, Chen X, Nan N, Bard J, Wu F, Yergeau D, Liu T, Wang J, Mu X (2023) Key transcription factors influence the epigenetic landscape to regulate retinal cell differentiation. Nucleic Acids Res 51:2151–2176.

Germain PL, Lun A, Garcia Meixide C, Macnair W, Robinson MD (2021) Doublet identification in single-cell sequencing data using scDblFinder. F1000Res 10:979.

Hao Y, et al. (2021) Integrated analysis of multimodal single-cell data. Cell 184:3573–3587.e29.

Harley RJ, Murdy JP, Wang Z, Kelly MC, Ropp TJF, Park SH, Maness PF, Manis PB, Coate TM (2018) Neuronal cell adhesion molecule (NrCAM) is expressed by sensory cells in the cochlea and is necessary for proper cochlear innervation and sensory domain patterning during development. Dev Dyn 247:934–950.

Hayashi S, McMahon AP (2002) Efficient recombination in diverse tissues by a tamoxifen-inducible form of Cre: a tool for temporally regulated gene activation/inactivation in the mouse. Dev Biol 244:305–318.

Hegazy M, Cohen-Barak E, Koetsier JL, Najor NA, Arvanitis C, Sprecher E, Green KJ, Godsel LM (2020) Proximity ligation assay for detecting protein-protein interactions and protein modifications in cells and tissues in situ. Curr Protoc Cell Biol 89:e115.

Huang EJ, Liu W, Fritzsch B, Bianchi LM, Reichardt LF, Xiang M (2001) Brn3a is a transcriptional regulator of soma size, target field innervation and axon pathfinding of inner ear sensory neurons. Development 128:2421–2432.

Kaya-Okur HS, Janssens DH, Henikoff JG, Ahmad K, Henikoff S (2020) Efficient low-cost chromatin profiling with CUT&Tag. Nat Protoc 15:3264–3283.

Kelley MW (2006) Regulation of cell fate in the sensory epithelia of the inner ear. Nat Rev Neurosci 7:837–849.

Kim WY, Fritzsch B, Serls A, Bakel LA, Huang EJ, Reichardt LF, Barth DS, Lee JE (2001) NeuroD-null mice are deaf due to a severe loss of the inner ear sensory neurons during development. Development 128:417–426.

Korsunsky I, Millard N, Fan J, Slowikowski K, Zhang F, Wei K, Baglaenko Y, Brenner M, Loh PR, Raychaudhuri S (2019) Fast, sensitive and accurate integration of single-cell data with harmony. Nat Methods 16:1289–1296.

Lanier J, Quina LA, Eng SR, Cox E, Turner EE (2007) Brn3a target gene recognition in embryonic sensory neurons. Dev Biol 302:703–716.

Li JY, Joyner AL (2001) Otx2 and Gbx2 are required for refinement and not induction of mid-hindbrain gene expression. Development 128:4979–4991.

Luo XJ, et al. (2013) GATA3 controls the specification of prosensory domain and neuronal survival in the mouse cochlea. Hum Mol Genet 22:3609–3623.

Ma Q, Chen Z, del Barco Barrantes I, de la Pompa JL, Anderson DJ (1998) Neurogenin1 is essential for the determination of neuronal precursors for proximal cranial sensory ganglia. Neuron 20:469–482.

Ma Q, Anderson DJ, Fritzsch B (2000) Neurogenin 1 null mutant ears develop fewer, morphologically normal hair cells in smaller sensory epithelia devoid of innervation. J Assoc Res Otolaryngol 1:129–143.

Maklad A, Fritzsch B (2002) The developmental segregation of posterior crista and saccular vestibular fibers in mice: a carbocyanine tracer study using confocal microscopy. Brain Res Dev Brain Res 135:1–17.

Mu X, Fu X, Beremand PD, Thomas TL, Klein WH (2008) Gene regulation logic in retinal ganglion cell development: isl1 defines a critical branch distinct from but overlapping with Pou4f2. Proc Natl Acad Sci U S A 105:6942–6947.

NIDCD (2013) Hearing aids. NIDCD Fact Sheet.
NIDCD (2016) Cochlear implants. In: *NIDCD fact sheet* (NIDCD, ed).
Ohyama T, Groves AK (2004) Generation of Pax2-Cre mice by modification of a Pax2 bacterial artificial chromosome. Genesis 38:195–199.
Pan L, Deng M, Xie X, Gan L (2008) ISL1 and BRN3B co-regulate the differentiation of murine retinal ganglion cells. Development 135: 1981–1990.
Petitpre C, Faure L, Uhl P, Fontanet P, Filova I, Pavlinkova G, Adameyko I, Hadjab S, Lallemend F (2022) Single-cell RNA-sequencing analysis of the developing mouse inner ear identifies molecular logic of auditory neuron diversification. Nat Commun 13:3878.
Pfaff SL, Mendelsohn M, Stewart CL, Edlund T, Jessell TM (1996) Requirement for LIM homeobox gene Isl1 in motor neuron generation reveals a motor neuron-dependent step in interneuron differentiation. Cell 84:309–320.
Radde-Gallwitz K, Pan L, Gan L, Lin X, Segil N, Chen P (2004) Expression of Islet1 marks the sensory and neuronal lineages in the mammalian inner ear. J Comp Neurol 477:412–421.
Ryan AF (1997) Transcription factors and the control of inner ear development. Semin Cell Dev Biol 8:249–256.
Schimmang T, Minichiello L, Vazquez E, Jose IS, Giraldez F, Klein R, Represa J (1995) Developing inner-ear sensory neurons require Trkb and Trkc receptors for innervation of their peripheral targets. Development 121: 3381–3391.
Sherrill HE, Jean P, Driver EC, Sanders TR, Fitzgerald TS, Moser T, Kelley MW (2019) Pou4f1 defines a subgroup of type I spiral ganglion neurons and is necessary for normal inner hair cell presynaptic Ca(2+) signaling. J Neurosci 39:5284–5298.
Shrestha BR, Chia C, Wu L, Kujawa SG, Liberman MC, Goodrich LV (2018) Sensory neuron diversity in the inner ear is shaped by activity. Cell 174:1229.
Skene PJ, Henikoff S (2017) An efficient targeted nuclease strategy for high-resolution mapping of DNA binding sites. Elife 6:e21856.
Steevens AR, Glatzer JC, Kellogg CC, Low WC, Santi PA, Kiernan AE (2019) SOX2 is required for inner ear growth and cochlear nonsensory formation before sensory development. Development 146:dev170522.
Sun YF, Dykes IM, Liang XQ, Eng SR, Evans SM, Turner EE (2008) A central role for Islet1 in sensory neuron development linking sensory and spinal gene regulatory programs. Nat Neurosci 11:1283–1293.
Sun YW, Wang LY, Zhu T, Wu BL, Wang GQ, Luo ZN, Li C, Wei W, Liu ZY (2022) Single-cell transcriptomic landscapes of the otic neuronal lineage at multiple early embryonic ages. Cell Rep 38:110542.
Thibodeau A, et al. (2021) AMULET: a novel read count-based method for effective multiplet detection from single nucleus ATAC-seq data. Genome Biol 22:252.
Torres M, Giráldez F (1998) The development of the vertebrate inner ear. Mech Dev 71:5–21.
van Arensbergen J, van Steensel B, Bussemaker HJ (2014) In search of the determinants of enhancer-promoter interaction specificity. Trends Cell Biol 24:695–702.
Xiang M, Gan L, Zhou L, Klein WH, Nathans J (1996) Targeted deletion of the mouse POU domain gene Brn-3a causes selective loss of neurons in the brainstem and trigeminal ganglion, uncoordinated limb movement, and impaired suckling. Proc Natl Acad Sci U S A 93:11950–11955.
Zou D, Silvius D, Fritzsch B, Xu PX (2004) Eyal and Six1 are essential for early steps of sensory neurogenesis in mammalian cranial placodes. Development 131:5561–5572.